Bioorganic & Medicinal Chemistry 17 (2009) 675–689

Contents lists available at ScienceDirect

Bioorganic & Medicinal Chemistry

journal homepage: www.elsevier.com/locate/bmc

New pyrazoline bearing 4(3*H*)-quinazolinone inhibitors of monoamine oxidase: Synthesis, biological evaluation, and structural determinants of MAO-A and MAO-B selectivity

Nesrin Gökhan-Kelekçi [a,*], Semra Koyunoğlu [b], Samiye Yabanoğlu [c], Kemal Yelekçi [d], Özen Özgen [e], Gülberk Uçar [c], Kevser Erol [f], Engin Kendi [e], Akgül Yeşilada [b]

[a] Hacettepe University, Faculty of Pharmacy, Department of Pharmaceutical Chemistry, 06100 Sıhhıye, Ankara, Turkey
[b] Hacettepe University, Faculty of Pharmacy, Department of Basic Pharmaceutical Sciences, 06100 Sıhhıye, Ankara, Turkey
[c] Hacettepe University, Faculty of Pharmacy, Department of Biochemistry, 06100 Sıhhıye, Ankara, Turkey
[d] Kadir Has University, The Faculty of Arts and Sciences, 34080 Fatih, İstanbul, Turkey
[e] Hacettepe University, Faculty of Engineering, Department of Physics Engineering, 06800 Beytepe, Ankara, Turkey
[f] Osmangazi University, Faculty of Medicine, Eskişehir, Turkey

ARTICLE INFO

Article history:
Received 7 July 2008
Revised 17 November 2008
Accepted 21 November 2008
Available online 3 December 2008

Keywords:
2-Pyrazoline
MAO-A/MAO-B inhibition
Docking
Antidepressant-anxiogenic activities
Crystallographic model

ABSTRACT

A new series of pyrazoline derivatives were prepared starting from a quinazolinone ring and evaluated for antidepressant, anxiogenic and MAO-A and -B inhibitory activities by in vivo and in vitro tests, respectively. Most of the synthesized compounds showed high activity against both the MAO-A (compounds **4a–4h, 4j–4n, and 5g–5l**) and the MAO-B (compounds **4i and 5a–5f**) isoforms. However, none of the novel compounds showed antidepressant activity except for **4b**. The reason for such biological properties was investigated by computational methods using recently published crystallographic models of MAO-A and MAO-B. The differences in the intermolecular hydrophobic and H-bonding of ligands to the active site of each MAO isoform were correlated to their biological data. Compounds **4i, 4k, 5e, 5i**, and **5l** were chosen for their ability to reversibly inhibit MAO-B and MAO-A and the availability of experimental inhibition data. Observation of the docked positions of these ligands revealed interactions with many residues previously reported to have an effect on the inhibition of the enzyme. Among the pyrazoline derivatives, it appears that the binding interactions for this class of compounds are mostly hydrophobic. All have potential edge-to-face hydrophobic interactions with F343, as well as π–π stacking with Y398 and other hydrophobic interactions with L171. Strong hydrophobic and H-bonding interactions in the MAO recognition of **4i** could be the reason why this compound shows selectivity toward the MAO-B isoform. The very high MAO-B selectivity for **4i** can be also explained in terms of the distance between the FAD and the compound, which was greater in the complex of MAO-A-**4i** as compared to the corresponding MAO-B complex.

1. Introduction

Inhibitors of monoamine oxidase have shown therapeutic value in a variety of neurodegenerative diseases.[1] The discovery in the 1950s of the antidepressant properties of MAO inhibitors (MAOIs) was the major finding that led to the monoamine theory of depression. Earlier MAO inhibitors introduced into clinical practice for the treatment of depression were abandoned due to adverse side-effects, such as hepatotoxicity, orthostatic hypotension and the so-called 'cheese effect' characterized by hypertensive crises.[2] This handicap was thought to be related to nonselective and irreversible monoamine oxidase inhibition. However, more recently, a better knowledge of the enzyme, in particular the identification of two isoforms (MAO-A and MAO-B) that can be selectively inhibited, and the development of new generations of inhibitors have led to a renewed interest in the therapeutic potential of these compounds. These two forms of MAO are characterized by their different sensitivities to inhibitors and their different specificities to substrates.[3] MAO-A preferably metabolizes serotonin, adrenalin, and noradrenalin,[4] whereas β-phenylethylamine and benzylamine are predominantly metabolized by MAO-B.[5] Tyramine, dopamine, and some other important amines are common substrates for both isoenzymes.[6]

Nowadays, the therapeutic interest of MAOIs falls into two major categories. MAO-A inhibitors have been used mostly in the treatment of mental disorders, in particular depression and anxiety,[7–9] while MAO-B inhibitors could be used in the treatment of Parkinson's disease and perhaps, Alzheimer's disease.[10,11] Despite

* Corresponding author. Tel.: +90 312 305 30 17; fax: +90 312 311 47 77.
E-mail address: onesrin@hacettepe.edu.tr (N. Gökhan-Kelekçi).

0968-0896/$ - see front matter © 2008 Elsevier Ltd. All rights reserved.
doi:10.1016/j.bmc.2008.11.068

the considerable progress in understanding the interactions of the two enzyme forms with their preferred substrates and inhibitors, few general rules are yet available for the rational design of potent and selective inhibitors of MAO-A and MAO-B. Despite these difficulties, efforts have been oriented toward the discovery of reversible and selective inhibitors of MAO-A/MAO-B leading to a new generation of compounds.

The recent determination of the crystal structure of the two isoforms of human MAO by Binda et al. elucidates the mechanism underlying the selective interactions between these proteins and their ligands, probes the catalytic mechanism, and provides a better understanding of the pharmacophoric requirements needed for a rational design of potent and selective enzyme inhibitors with a therapeutic potential.[12–15]

The classical period of the MAO inhibitors started with hydrazine derivatives. Originally proposed as a tuberculostatic agent, their prototype, iproniazid, was the first modern antidepressant and was introduced into the market under the trade name Marsilid®.[16] Subsequently, research has been directed at the preparation of heterocyclic hydrazines and hydrazides and their potential as therapeutic agents for the treatment of CNS depression.[17–19]

2-Pyrazolines can be considered as a cyclic hydrazine moiety. For this reason, some authors investigated MAO-inhibitory properties of 1,3,5-triphenyl-2-pyrazolines and found high activity.[20–27] The discovery of this class of drugs has led to a considerable increase in modern drug development in this area and has also pointed out the unpredictability of biological activity from structural modification for a prototype drug molecule.

All these findings have pushed us to synthesize various pyrazoles derivatives and examine their different amine oxidase inhibition activities including bovine serum amine oxidase (BSAO), MAO, and semicarbazide sensitive amine oxidase (SSAO). A considerable number of the prepared compounds were found to have BSAO, SSAO, and MAO-inhibitory activity comparable to or higher than the reference compounds.[28–30] At the same time, some of the pyrazoles, which were presented as selective MAO-B inhibitors,[24] were found to inhibit the AChE activities of human erythrocyte and plasma, approved for the treatment of cognitive dysfunction in AD, selectively, and noncompetetively[31] (Fig. 1).

Moreover, a number of quinazolinones and their analogues have shown clinical importance through the exhibition of monoamine oxidase inhibitory activity. It was observed that the 2nd and 3rd positions of quinazolinones have been the target for the substitution of different heterocyclic moieties.[32–36] However, a 5-membered pyrazoline ring has not appeared to be linked with quinazolinones so far. These observations motivated us to link different heterocyclic moieties to synthesize a new series of pyrazole derivatives by combining the quinazolinone moiety at the 1st position in order to evaluate the effect of this substitution on monoamine oxidase inhibitory effects.

2. Results and discussion

To verify the effects of structural modifications on both inhibition and selectivity toward MAO-A/MAO-B, and antidepressant and anxiogenic activities of 26 2-(1′-substituted phenyl-3′-heteroaryl-2′-propenylidene)hydrazine-3-methyl-4(3*H*)-quinazolinone and 2-(3-substituted phenyl-5′-heteroaryl-2′-pyrazoline-1-yl)-3-methyl-4(3*H*)-quinazolinone derivatives, 12 new ones have been synthesized. In particular, the influence on biological behavior (such as MAO inhibition, antidepressant, and anxiogenic activities) of the introduction of different aromatic rings in the 3 and 5 positions of the 4,5-dihydro-(1*H*)-pyrazole nucleus containing 3-methyl-4(3*H*)-quinazolinone has been investigated.

2.1. Chemistry

We described here a convenient approach to the preparation of 2-(1′-substituted phenyl-3′-heteroaryl-2′-propenylidene)hydrazine-3-methyl-4(3*H*)-quinazolinone and 2-(3-substituted phenyl-5′-heteroaryl-2′-pyrazoline-1-yl)-3-methyl-4(3*H*)-quinazolinone **4a–4f/5a–5f**. For the synthesis of the desired compounds, Scheme 1 was followed.

The key reactions involved are the intermediate formation of hydrazones and subsequent addition of N–H on the olefinic bond of the propenone moiety that form the ring-closed final products **5**. In the ^{1}H NMR spectra of the compounds **4**, olefinic protons (2′-CH and 3′-CH) appeared as doublets at about 6.8 and 7.8 ppm, respectively (J_{trans} = 14–16 Hz). After the ring closure, ring protons (H_A and H_B) of the compounds **5** showed at around 3.4 and 3.7 ppm and also H_X gave triplet/multiplet at about 6.3 ppm due to vicinal coupling with the two magnetically nonequivalent protons of the methylene group. The quinazolinone and phenyl protons were observed at the expected chemical shifts and integral values. In the IR spectra of the compounds **5a–5f** the disappearance of C=C (olefinic) and N–H stretching bands at 1584–1608 and 3257–3366 cm^{-1} is due to the ring closure.

The characteristic peaks were observed in the mass spectra of the compounds. Molecular ion peaks (M^+) provided the molecular formula of all synthesized compounds **4a–4f/5a–5f**. Characteristic M+2 isotope peaks were observed in the mass spectra of the compounds having a halogen or a sulfur. As for the compounds **5a–5f**, the 2-pyrazoline moiety have shown a fragmentation pattern giving rise to desired peaks at *m*/*e* 250, 252, 268, and 282 (Scheme 2).

The fragmentation of compounds **4a–4f** occurs via cleavage of quinazolinone moiety from the other group giving desired peaks at *m*/*z* 159. This is followed by the loss of a C_2H_2N radical to produce an ion at *m*/*z* 119 (Scheme 3).

2.2. X-ray crystal analysis of 5a

A colorless suitable crystal with dimensions 0.42 × 0.48 × 0.48 mm was chosen for the structure determination. The diffraction intensity data were collected at room temperature on an Enraf-Nonius CAD-4 diffractometer using graphite-monochromated radiation (Cu Kα, λ = 1.54184 Å). *w*/2*θ* scan mode was employed for data collection. The cell parameters were refined from accurately determined 25 reflections in the range of 3.7° ⩽ *θ* ⩽ 74.2°. A total of 4320 reflections (4128 unique, 3088 observed [$I > 2\sigma(I)$]) were col-

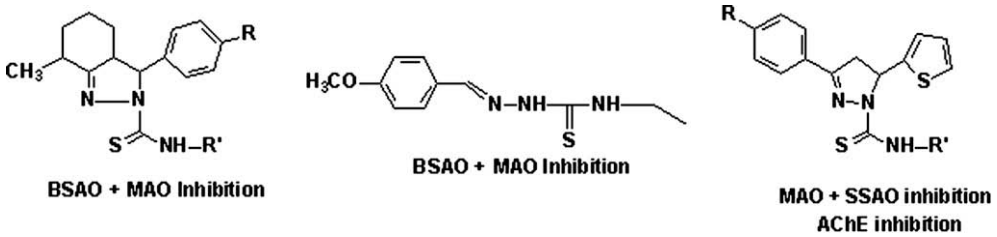

Figure 1. Pyrazole derivatives having MAO, SSAO, and BSAO inhibition.

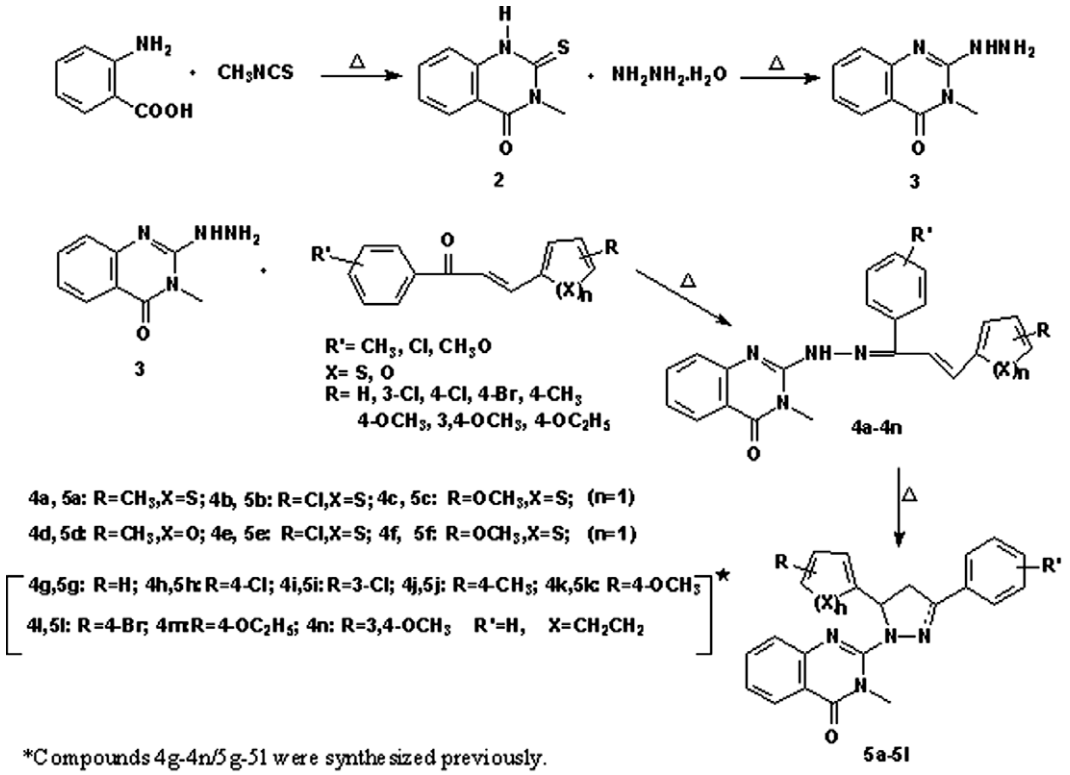

Scheme 1. Synthetic pathway of compounds **4a–4n**/**5a–5i**.

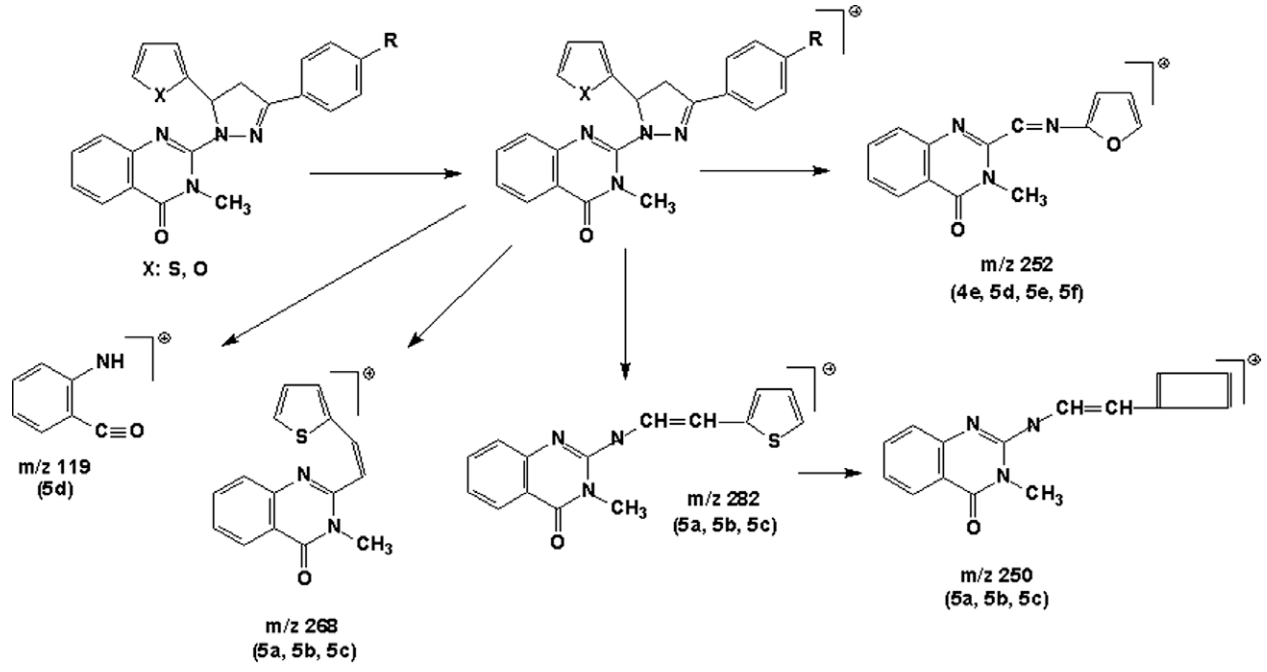

Scheme 2. Fragmentation pattern of the compounds (**5a–5f**).

lected for $-11 \leqslant h \leqslant 11, -12 \leqslant k \leqslant 11, 0 \leqslant l \leqslant 16$ with $R_{int} = 0.0148$. Extinction correction was not applied.

The crystal structure was solved by direct methods using the SHELXS-97 program[37] which revealed the positions off all the non-hydrogen atoms and these were refined isotropically and then anisotropically by full matrix least-squares calculations (based on $|F^2|$) using SHELXL-97.[38] The experimental crystallographic data and refinement parameters are given in Table 1.

All hydrogen atoms were positioned geometrically and refined using a riding model with (C–H (aromatic) = 0.93, 97, 98, and 0.96 Å for methyl H atoms). After a few cycle refinements, an empirical Ψ scan absorption correction was applied.[39] The view of the molecule performed using ORTEP[40] and some selected bond lengths, angles, and torsion angles are given in Figure 2.

The 2-pyrazoline ring deviates markedly from planarity with the torsion angles N1–C12–C11–C10 of 15.6(3)°. The pyrazoline

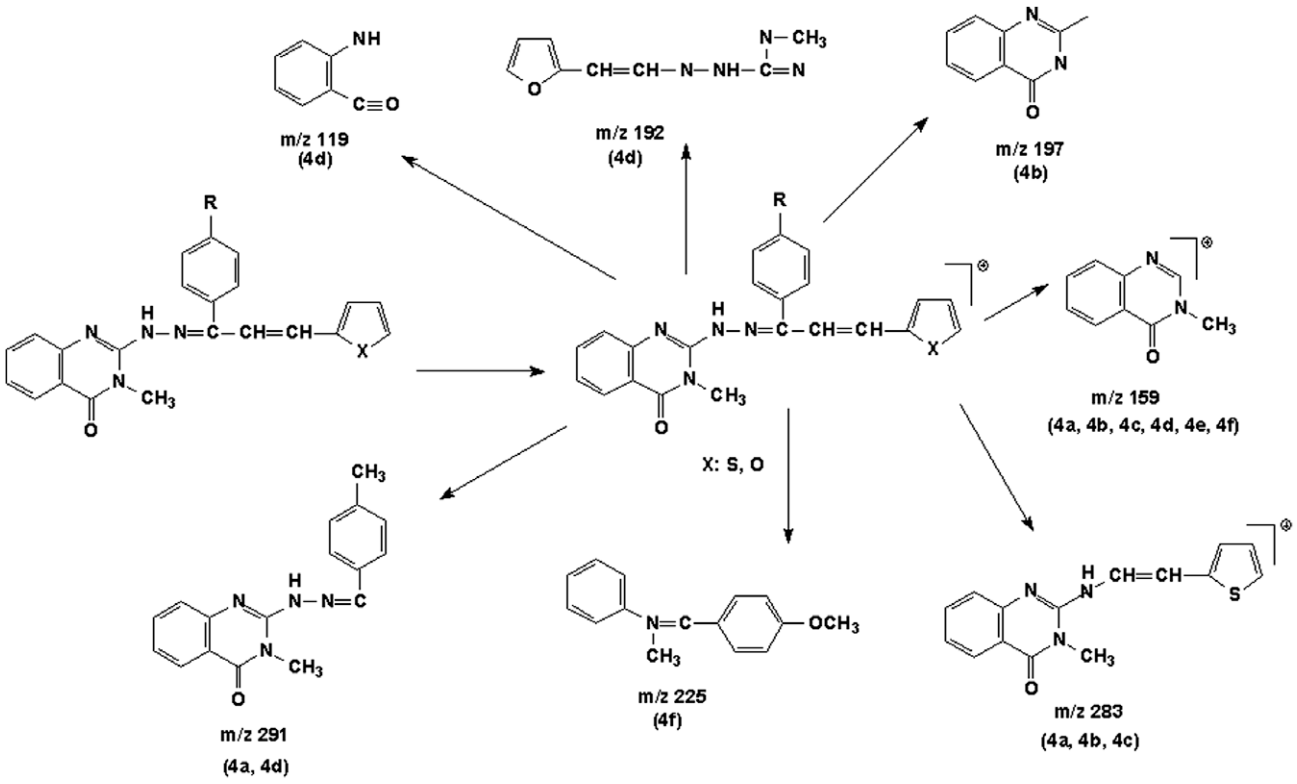

Scheme 3. Fragmentation pattern of the compounds (**4a**–**4f**).

Table 1
Crystallographic and refinement parameters of the molecule

Molecular formula	$C_{23}H_{20}N_4OS$
Formula weight	400.50
Temperature (K)	293 (2)
Wavelength (Å)	1.54184
Crystal system	Triclinic
Space group	$P\bar{1}$
Cell dimensions	
a (Å)	8.889 (2)
b (Å)	9.838 (3)
c (Å)	12.871 (3)
α (°)	110.86 (2)
β (°)	92.35 (2)
γ (°)	100.15 (2)
Volume (Å^3)	1028.9 (5)
Z	2
Density (calculated) (Mg m^{-3})	1.36
Absorption coefficient (mm^{-1})	1.564
F_{000}	420
Crystal size (mm)	0.42 × 0.48 × 0.48
Crystal color	Colorless
θ range for data collection (°)	3.7–74.2
Index ranges	$-11 \leqslant h \leqslant 11$
	$-12 \leqslant k \leqslant 11$
	$0 \leqslant l \leqslant 16$
Reflections collected	4320
Independent reflections	4128 [R_{int} = 0.0148]
Refinement method	Full-matrix least-squares on F^2
Data/restraints/parameters	4128/0/262
Goodness-of-fit on F^2	1.055
R indices [$I > 2\sigma(I)$]	R_1 = 0.065, wR_2 = 0.194
(Δ/σ)	0
$\Delta\rho_{max}$ (eÅ^{-3})	0.574
$\Delta\rho_{min}$ (eÅ^{-3})	−0.531

ring is in a distorted envelope conformation. Maximum deviation of the C12 atom from the N1–N2–C10–C11 plane is 0.283(3) Å. The bond lengths and angles of the pyrazoline ring are compared

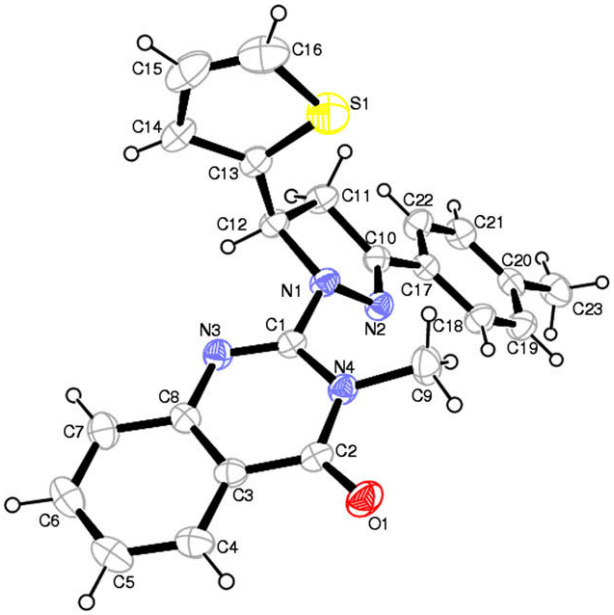

Figure 2. QRTEP drawing of the molecule indicating atom numbering scheme with 30% probability. Selected intramolecular bond lengths (A), bond angles (°) and torsion angles (°) of **5a** SI–C16 = 1.678(4). S1–C13 = 1.691(3), C13–C14 = 1.457(4), C15–C16 = 1.311(7), N1–N2 = 1.416(3) N2–C10 = 1.288(4), C10–C11 = 1.503(4), C12–C11 = 1.534(4). N1–C12 = 1.488(3), C12–C13 = 1.501(4), N4–C3 = 1.470(4). N3–C3 = 1.390(4), N4–C2 = 1.387(4), N3–C1 = 1.283(3), C1–C2 = 1.230(3), C13–S1–C16 = 92.6(2), S1–C16–C15 = 112.7(3), C16–C15–C14 = 116.4(4), C15–C14–C13 = 106.5(3), C14–C13–S1 = 111.7(2), N1–N2–C10 = 108.4(2), N2–C10–C11 = 113.5(2). C10–C11–012 = 102.9(2), C11–C12–N1 = 101.1(2). C12–N1–N2 = 110.9(2), C11–C10–C17 = 125.1(2), C13–C12–N12 = 109.8(2), C13–C12–C11 = 116.1(2), C1–N1–C12 = 118.8(2), C1–N1–N2 = 113.9(2), O1–C2–N4 = 120 0(3), N1–C1–N3 = 119.2(2), N4–C1–N1 = 115.7(2), S1–C13–C14–C15 = 17(3). N1–N2–C10–011 = −1.1(3). C10–C11–C12–N1 = 15.6(3). C1–N4–C2–O1 = −179.3(3), S1–C13–C12–N1 = 53.3(3), C10–C11–C12–C13 = 134.4(3), N2–N1–C12–C13 = −141.0(2), N2–C10–C17–C22 = 173.3(3), N2–N1–C1–N4 = 617(3).

with the corresponding values of similar compounds.[41,27] In the present study, all the geometric parameters of the pyrazoline ring are in agreement with the reported values in 2-[3-phenyl-5-(*m*-chlorophenyl)-2-pyrazolin-1-yl]-3-methyl-4(3*H*)-quinazolinone[41] and a new therapeutic approach in the treatment of Alzheimer disease: some novel pyrazole derivatives as a dual MAO-B inhibitors and antiinflammatory analgesics.[27]

The 4(3*H*)-quinazolinone group attached to the N1 atom. The N1–N2 bond shows a single bond character with the value of 1.416(3) Å. The N1–N2 bond length is almost similar to the values of 1.411(7) and 1.413(7) Å reported in 2-[3-phenyl-5-(*m*-chlorophenyl)-2-pyrazolin-1-yl]-3-methyl-4(3*H*)-quinazolinone[41] and the value of 1.400(2) Å reported in a new therapeutic approach in Alzheimer disease: some novel pyrazole derivatives as a dual MAO-B inhibitors and antiinflammatory analgesics.[27]

The N2–C10 [1.288(4) Å] and N1–C12 [1.488(3) Å] bonds are well in agreement with the values of 1.285(2) and 1.483(2) Å reported in 1′,2′,3′,4′-tetrahydro-1,3-diphenyl-4-chlorospiro[2-pyrazoline-5,2-napthalen]1′one.[42]

Whereas the 3-methyl-4(3*H*)-pyrimidine ring deviates slightly from the planarity, the phenyl ring of the quinazolinone moiety adopts nearly planar conformation. The C3 atom deviates from the plane of the pyrimidine ring with the distance of −0.0314(2) Å.

The ketone group located C2 is in the same plane with the pyrimidine structure with a C1–N4–C2–O1 torsion angle of −179.3(3)°. The C1–N3 [1.283(3) Å] and C2–N4 [1.387(4) Å] bond lengths are in agreement with the values of 1.277(8) and 1.277(8) Å and 1.401(9) and 1.408(9) Å reported for 2-[3-phenyl-5-(*m*-chlorophenyl)-2-pyrazolin-1-yl]-3-methyl-4(3*H*)-quinazolinone.[41]

In the thienyl ring, though the C15–C16 [1.311(7) Å] bond shows a double bond character and is shorter than the values of 1.339(3) and 1.365(3) Å reported for 3-phenyl-5(2-thienyl)-2-pyrazoline-1-thioamide,[43] the C13–C14 [1.457(4) Å] bond shows a single bond character. The S1–C13 [1.691(3)Å] and S1–C16 [1.678(4) Å] bonds are in agreement with the values reported for 3-phenyl-5(2-thienyl)-2-pyrazoline-1-thioamide [S1–C10 = 1.703 (2) and S1–C13 = 1.716(2) Å].[43] The thienyl ring is almost perpendicular to the pyrazoline ring. The dihedral angle between two rings is 84.8(1)°. The dihedral angle between the pyrazoline ring and the phenyl ring is 6.7(1)° and these rings are nearly coplanar. The determination of the structure indicates the absolute *R* configuration of the chiral atom C12.

Furthermore van der Waals forces, the crystal packing is stabilized by C–H···O and C–H···N intramolecular interactions [for C9–H9A···O1; D–H = 0.96, H...A = 2.23, D...A = 2.688(5), D–H...A = 108 [for C9–H9A···N2; D–H = 0.96, H...A = 2.34, D...A = 2.909(5), D–H...A = 117].

2.3. Biochemistry

MAO-A and MAO-B inhibitory activities of newly synthesized 4(3*H*)-quinazolinone derivatives were determined using MAO isoforms of rat liver (Table 2). Liver tissue was used to screen the MAO-inhibitory actions of these novel compounds since liver was reported to be a good source for both isoforms of the enzyme.

According to the IC_{50} values corresponding to the inhibition of rat liver MAO-A and -B by the newly synthesized quinazolinone derivatives, compounds **2, 4a–4h, 4j–4n**, and **5g–5l** inhibited rat

Table 2
Kinetic data corresponding to the inhibition of rat liver MAO isoforms by the newly synthesized quinazoline derivatives[a]

Compound	K_i values[a] (μM) for MAO-A	IC_{50} for MAO-A (μM)[b] preincubation 60 min	K_i values[a] (μM) for MAO-B	IC_{50} for MAO-B (μM)[b] preincubation 60 min	MAO-inhibitory selectivity
4a	190.12 ± 10.26	33.16 ± 2.50	188.22 ± 9.80	419.12 ± 33.25	Selective for MAO-A
4b	28.16 ± 1.50	28.05 ± 3.56	69.12 ± 5.01	415.70 ± 17.19	Selective for MAO-A
4c	185.13 ± 12.16	27.18 ± 1.76	184.40 ± 12.00	299.30 ± 21.25	Selective for MAO-A
4d	180.80 ± 11.10	90.80 ± 8.63	179.11 ± 10.05	320.34 ± 21.20	Selective for MAO-A
4e	80.13 ± 5.16	31.60 ± 2.80	125.13 ± 10.55	400.05 ± 23.35	Selective for MAO-A
4f	70.26 ± 6.48	34.20 ± 2.76	90.55 ± 7.89	419.30 ± 26.76	Selective for MAO-A
4g	34.20 ± 2.60	35.10 ± 3.90	70.55 ± 5.80	415.20 ± 40.85	Selective for MAO-A
4h	1.05 ± 0.95	3.56 ± 0.28	7.80 ± 0.67	377.75 ± 16.98	Selective for MAO-A
4i	5.10 ± 0.23	468.00 ± 20.66	0.16 ± 0.08	1.15 ± 0.12	Selective for MAO-B
4j	30.16 ± 0.17	30.50 ± 1.90	64.56 ± 5.32	470 ± 27.16	Selective for MAO-A
4k	1.15 ± 0.10	9.05 ± 0.18	10.58 ± 1.19	399.00 ± 19.00	Selective for MAO-A
4l	40.27 ± 3.05	30.50 ± 1.90	69.57 ± 5.54	487.05 ± 47.83	Selective for MAO-A
4m	80.11 ± 6.13	29.00 ± 2.50	30.56 ± 2.75	429.00 ± 28.50	Selective for MAO-A
4n	90.67 ± 8.40	68.01 ± 5.88	65.12 ± 5.18	470.50 ± 30.00	Selective for MAO-A
5a	130.45 ± 10.77	414.75 ± 34.00	90.68 ± 7.47	70.83 ± 7.16	Selective for MAO-B
5b	65.33 ± 5.13	420.23 ± 27.21	25.56 ± 1.96	27.56 ± 1.36	Selective for MAO-B
5c	25.28 ± 2.01	439.93 ± 30.18	16.27 ± 1.20	15.23 ± 1.60	Selective for MAO-B
5d	140.23 ± 10.44	410.11 ± 17.59	88.56 ± 7.16	77.13 ± 6.98	Selective for MAO-B
5e	28.74 ± 2.05	450.24 ± 30.55	9.25 ± 0.71	7.22 ± 0.70	Selective for MAO-B
5f	6.80 ± 0.52	418.00 ± 20.20	1.48 ± 0.66	2.03 ± 0.27	Selective for MAO-B
5g	9.90 ± 0.80	9.46 ± 0.72	25.20 ± 1.99	409.76 ± 10.70	Selective for MAO-A
5h	2.70 ± 0.20	3.70 ± 0.27	18.43 ± 1.60	415.70 ± 17.19	Selective for MAO-A
5i	0.90 ± 0.07	1.02 ± 0.09	5.80 ± 0.75	399.90 ± 12.30	Selective for MAO-A
5j	2.56 ± 0.31	4.51 ± 0.33	7.90 ± 0.52	483.77 ± 36.50	Selective for MAO-A
5k	1.03 ± 0.10	4.51 ± 0.33	9.90 ± 0.81	400.22 ± 20.89	Selective for MAO-A
5l	1.17 ± 0.19	1.68 ± 0.18	10.55 ± 0.89	485.26 ± 26.71	Selective for MAO-A
2	30.18 ± 1.97	3.42 ± 0.47	78.34 ± 5.09	120.35 ± 11.60	Selective for MAO-A
3	25.23 ± 2.46	37.41 ± 2.05	18.58 ± 1.25	21.16 ± 6.83	Selective for MAO-B
Pargyline	**8.50 ± 0.89**	390.20 ± 17.23	**3.36 ± 0.27**	3.85 ± 0.23	Selective for MAO-B
Clorgyline	**1.20 ± 0.09**	2.05 ± 0.19	**5.60 ± 0.44**	400.90 ± 15.54	Selective for MAO-A
Selegiline	**15.70 ± 1.04**	499.01 ± 18.20	**1.35 ± 0.12**	2.01 ± 0.15	Selective for MAO-B
Moclobemide	**5.53 ± 0.27**	3.90 ± 0.19	**10.21 ± 0.83**	480.12 ± 21.05	Selective for MAO-A

[a] K_i values were determined from the kinetic experiments in which *p*-tyramine was used at 500 μM to measure MAO-A and 2.5 mM to measure MAO-B. Pargyline or clorgyline were added at 0.50 μM to determine the isoenzymes A and B. Newly synthesized compounds and the known inhibitors were preincubated with the homogenates for 60 min at 37 °C.

[b] IC_{50} values were determined from plots of residual activity percentage, calculated in relation to a sample of the enzyme treated under the same conditions without inhibitor, versus inhibitor concentration [I]. Newly synthesized compounds and the known inhibitors were preincubated with the homogenates for 60 min at 37 °C.

liver MAO-A selectively while compounds **3, 4i**, and **5a–5f** inhibited rat liver MAO-B selectively (Table 2).

These compounds were found to be time-dependent inhibitors of MAO-A since their inhibitory activities were significantly increased parallel to the increased incubation time. Homogenates were preincubated with the compounds for 0, 10, 20, 40, and 60 min (Table 2). After 60 min of preincubation, activity was found to be unchanged and the most potent inhibitory activities of these compounds were found by incubation at 37 °C for 60 min.

The starting compound entitled quinazolinone ring (compound **2**) inhibited MAO-A competitively and reversibly whereas quinazolinone hydrazine (compound **3**) inhibited MAO-B competitively and irreversibly with the K_i values of 30.18 ± 1.97 and 18.58 ± 1.25 μM, respectively.

Hydrazone derivatives bearing quinazolinone ring, compounds **4a–4n** except that **4i**, were found as selective MAO-A inhibitors irrespective of the substituents with the K_i values of 190.12 ± 10.26; 28.16 ± 1.50; 185.13 ± 12.16; 180.80 ± 11.10; 80.13 ± 5.16; 70.26 ± 6.48; 34.20 ± 2.60; 1.05 ± 0.95; 0.16 ± 0.08; 30.16 ± 0.17; 1.15 ± 0.10; 40.27 ± 3.05; 30.56 ± 2.75; and 65.12 ± 5.18 μM, respectively. Compounds **4a–4g** inhibited MAO irreversibly in a noncompetitive manner whereas compounds **4h–4l** inhibited MAO irreversibly in a competitive manner.

These results suggested that substitutions on quinazolinone hydrazone prevent the interaction of the molecule with the compact active site of MAO-B, but, contrarily, may enable the interaction of the compounds with the relatively larger catalytic cavity of MAO-A. Quite the opposite of these, compound **4i** acted as a selective MAO-B inhibitor with a K_i value of 0.16 ± 0.08 μM in a competitive and reversible manner.

It seemed that the compounds bearing phenyl moiety at the 3 position and substituted phenyl at the 5 position (compounds **4g–4n**) were more effective than those which carried substituted phenyl at the 3 position and furyl/thienyl at the 5 position. The main difference in the MAO-inhibitory activities of these compounds seemed to originate from the replacement of the methyl, bromo, ethoxy, and 3,4-dimethoxy on the aromatic moiety at the 5 position by a chloride atom or a methoxy group. The position of chloride on the phenyl ring of the molecule seems to be responsible for the MAO-inhibitory activity since compound **4i**, which has a chloride at *m*-position of the phenyl ring inhibits MAO-B potently while *p*-chloride derivatives inhibit MAO-A (Tables 2 and 3).

o-Chloride substitution may block the compounds' fit in the narrow active cavity of the MAO-B molecule.

Compounds **5a**, **5b**, and **5c** carrying thienyl moiety and **5d**, **5e**, and **5f** carrying furyl moiety at fifth position of the molecule inhibited MAO-B competitively and reversibly with the K_i values of 90.68 ± 7.47; 25.56 ± 1.96; 16.27 ± 1.20; 88.56 ± 7.16; 9.25 ± 0.71; and 1.48 ± 0.66 μM, respectively. The most potent compound in this group was compound **5f**, which bears a methoxy group on the phenyl at 3 position of the pyrazoline and furyl at its 5 position.

Compounds **5g**, **5h**, **5i**, **5j**, **5k**, and **5l**, which have a phenyl and substituted phenyl at 3 and 5 positions, respectively, inhibited MAO-A competitively and reversibly (Table 3). The most potent inhibitor in this group was compound **5i**, which bears a chloride group at 3 position on the phenyl ring (Table 2 and Fig. 3).

As a result, it is worth noting that the main difference in the MAO-inhibitory activities of pyrazoline type compounds **5a–5l** is found when the 5-membered heterocycle at the fifth position of the pyrazoline ring is replaced by a 6-membered heterocycle. This replacement appeared to be responsible for the remarkable differences in the inhibition activity mainly against MAO-A/MAO-B isoforms, respectively.

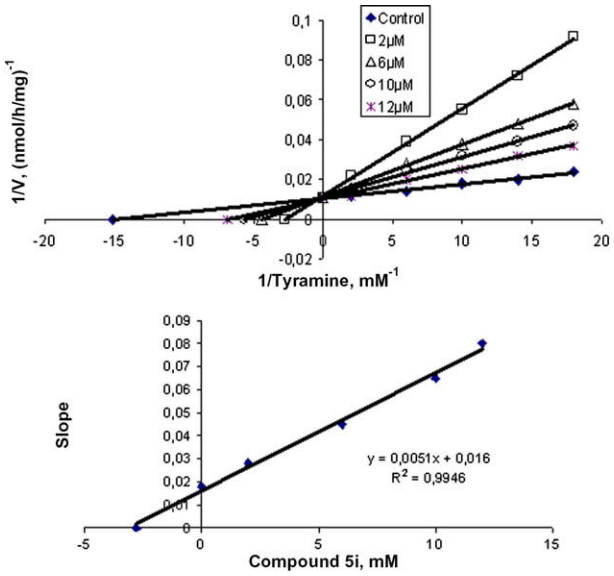

Figure 3. Lineweaver-Burk plot for the inhibition of rat liver MAQ-A by the compound **5i** (2–20 μM) with 60 min of preincubation at 37 °C. *p*-Tyramine was used as substrate in the concentration range of 50–500 μM. Value are means of the independent experiments. *Equations corresponding to the lines at the first graph are $y = 0.0044x + 0.012$ $R^2 = 0.3990$ for 10 μM inhibitor; $y = 0.0026x + 0.0114$ $R^2 = 0.9968$ for 10 μM inhibitor; $0.0015x + 0.0103$ $R^2 = 0.9968$ for 12 μM inhibitor; and 0.007×0.0106 $R^2 = 0.9950$ for control. **Second graph represents the plot of the slope of reciprocal plot.

Table 3
Calculated and experimental K_i values for the inhibition of rat liver MAO isoforms of the selected quinazoline derivatives

Compound	Experimental K_i values* (μM)	Calculated K_i values for MAO-A (μM)	Calculated K_i values for MAO-B (μM)	Inhibition type
4h	1.05 ± 0.95 (for MAO-A)	0.088	2.45	Selective for MAO-A competitive reversible
4i	0.16 ± 0.08 (for MAO-B)	0.020	0.36 (nM)	Selective for MAO-B competitive reversible
4k	1.15 ± 0.10 (for MAO-A)	0.045	2.57	Selective for MAO-A competitive reversible
5e	9.25 ± 0.7 (for MAO-B)	6.41	3.74	Selective for MAO-B competitive reversible
5f	1.48 ± 0.22 (for MAO-B)	0.94	0.98	Selective for MAO-B competitive reversible
5g	9.90 ± 0.80 (for MAO-A)	37.31	79.96	Selective for MAO-A competitive reversible
5h	2.70 ± 0.20 (for MAO-A)	2.12	58.53	Selective for MAO-A competitive reversible
5i	0.90 ± 0.07 (for MAO-A)	0.79	0.96	Selective for MAO-A competitive reversible
5j	2.56 ± 0.31 (for MAO-A)	2.5	12.6	Selective for MAO-A competitive reversible
5k	1.03 ± 0.10 (for MAO-A)	0.25	10.33	Selective for MAO-A competitive reversible
5l	1.17 ± 0.19 (for MAO-A)	0.57	583	Selective for MAO-A competitive reversible
2	30.18 ± 1.97 (for MAO-A)	48.63	39.89	Selective for MAO-A competitive reversible
3	18.58 ± 1.25 (for MAO-B)	23.78	19.08	Selective for MAO-B competitive irreversible

* K_i values were determined from the kinetic experiments in which *p*-tyramine was used at 500 μM to measure MAO-A and 2.5 mM to measure MAO-B. Pargyline or clorgyline were added at 0.50 μM to determine the isoenzymes A and B. Newly synthesized compounds and the known inhibitors were preincubated with the homogenates for 60 min at 37 °C. Each value represents means ± SEM of three independent experiments.

2.4. Molecular docking studies

In order to gain more insight into the binding mode and obtain additional validations for a few unexpected results, molecular docking studies were also performed for the compounds (**4i, 4k, 5e, 5i, 5l, 13, and 14**) experimentally tested. The calculated inhibition constants (K_i) as well as their experimental values for each enzyme–inhibitor complex are shown in Table 3. In general, the results obtained computationally are in good agreement with the experimental values. All compounds experimentally tested were found to be MAO-A selective except compounds **4i**, **5e**, **5f**, and **14** which were found to be MAO-B selective. These results were supported by the computational modeling studies. The exception to this was compound **2** which showed slightly higher MAO-B activity. The compound **5f** showed the same potency toward both MAO-A and MAO-B. In order to see the binding pose of these types of compounds in detail five representative ligands **4i**, **4k**, **5e**, **5i**, and **5l** were chosen.

Figure 4a–c shows the binding mode of compound **4i** in the MAO-B binding cavity. To date **4i** shows the highest MAO-B potency (K_i = 363 pmol) among the compounds tested in this study. Analysis of the docking results of compound **4i** in complex with MAO-B revealed that the 4(3*H*)-quinazolinone ring system of the ligand was inserted into the hydrophobic aromatic cage surrounded by FAD, Tyr435, and Tyr398. The inhibitor snugly fits the active site making various close contacts with the active site residues. One important interaction between **4i** and MAO-B indicates a strong stabilizing hydrogen bond between the azo group hydrogen next to quinazolinone ring and the backbone carbonyl of Ile 199 [1.76 Å Fig. 4a and c].

The lack of this hydrogen bond between **4i** and MAO-A makes this inhibitor 56-fold more selective toward MAO-B as a result of this computational work. The 4(3*H*)-quinazolinone ring of the inhibitor makes some important van der Waals interactions with FAD (2.43 Å), Tyr435 (2.61 Å), Tyr398 (3.97 Å), Cys172 (2.61 and 3.23 Å). Gln206 plays an important role in this inhibition, contributing two important interactions (2.64 Å between carbonyl of the Gln206 and N1 nitrogen of the 4(3*H*)-quinazolinone ring and 2.87 Å between the azo group of the ligand and side chain of Gln206). Phe343 (4.15 Å), Tyr326 (3.28 Å), Leu171 (3.48 Å), Phe168 (3.28 Å), and Ile199 (3.03 Å) are the other residues making close interactions resulting high inhibition potency (Fig. 4a and b). On the other hand **4i** is oriented differently in the active site of MAO-A than that of MAO-B in Figure 4d and e. The 4(3*H*)-quinazolinone ring system of the ligand is not sandwiched between Tyr407 (3.67 Å) and Tyr444 (3.11 Å) and it is not as close to FAD (2.79 Å) like in MAO-B causing low potency (K_i = 0.020 μM). This value is much lower potency than that of **4i** in MAO-B (K_i = 0.36 nM). The other contributing van der Waals interactions are between the residues of Phe352 (3.04 Å), Asn181 (4.72 Å), Cys323 (3.37 Å), and Val210 (3.06 Å) and the various atoms of the inhibitor shown in Figure 4d and e.

The binding mode of the compound **4k** with MAO-A observed at the end of docking simulation was shown in Figure 5a.

It is interesting to see that the phenyl moiety in **4k** was sandwiched between Tyr407 (a distance of 3.43 Å) and Tyr444 (a distance of 3.58 Å). The methoxy phenyl group is in close proximity with Glu216 (a distance of 2.79 Å). The other important van der Waals interactions between the **4k** and the various residues are Phe352 (a distance of 3.10 Å), Ile355 (a distance of 3.54 Å), Phe208 (a distance of 3.794.85 Å) and Cys323 (a distance of 3.12 Å). In Figure 5b, the docked mode of compound **4k** with MAO-B was shown.

The 4(3*H*)-quinazolinone ring was oriented across Tyr398 and Tyr435 making one important hydrogen bond between the carbonyl group at the 4 position of 4(3*H*)-quinazolinone and hydroxyl hydrogen of Tyr435 (1.94 Å). Cys172 (a distance of 2.90 Å), Leu171 (a distance of 2.59 Å), Tyr326 (a distance of 2.51 Å), and Ile199 (a distance of 3.54 Å) are the other close contact residues in the active site. Varying degrees of electrostatic and van der Waals interactions may contribute to the binding and stabilization of **4k** with MAO-A at almost two order of magnitude better than MAO-B.

The binding mode of inhibitor **5e** within the MAO-A cavity is shown in Figure 6a. The chlorophenyl group of **5e** was sandwiched between Tyr444 (4.35 Å), Tyr407 (5.50 Å), and FAD (4.04 Å). Ile335, Gln215, Val210, and Cys323 are the other residues in the active site, however, they are not contributing much to the binding and stabilization of **5e**.

Figure 6b shows the optimal binding mode of **5e** in the active site of the MAO-B. The chlorophenyl group of **5e** was inserted much further into the hydrophobic cage, lined with Tyr398 (4.20 Å) and Tyr435 (4.16 Å), than that of MAO-A. Gln206 (4.10 Å) and Tyr326 (3.56 Å) are interacting with N2 nitrogen of the pyrazole ring. The other important interactions between **5e** and the side chains of Ile199 (2.28 Å) and Thy326 (3.56 Å) have considerable effect on the inhibitions of this compound. The effective binding mode of **5e** with MAO-B makes this compound a better MAO-B inhibitor than MAO-A.

Figure 7a shows the binding modes of compound **5i** (**a**) into the MAO-A binding cavity and (**b**) into the MAO-B binding cavity. A close look at the docking results of compound **5i** in complex with MAO-A shows that its chlorophenyl group at the 3 position of the pyrazole ring complexed with MAO-A shows that its chlorophenyl group at 3 position of the pyrazole ring inserted between Tyr407, Tyr444, and the FAD hydrophobic region. It was seen that the Cl atom of the inhibitor is making important van der Waals interactions with the hydroxyl group of the side chain of Tyr407 (3.72 Å), Tyr444 (6.62 Å), and FAD (3.55 Å). Hydroxyl group of Glu216 is interacting very closely with the N2 nitrogen of the pyrazole ring (2.31 Å). The phenyl moiety of the Phe352 is in close proximity (2.95 Å) to chlorophenyl group at 3 position of the pyrazole ring making π–π interaction. The 4(3*H*)-quinazolinone ring system of the ligand was positioned in the entrance cavity making some van der Waals interactions with Phe209 (4.05 Å), Cys323 (2.90 Å), and Ile355 (3.63 Å).

Contrary to this pose, the same ligand was oriented in MAO-B in an upside down position in Figure 7b. Its 4(3*H*)-quinazolinone ring inserted into the 'aromatic cage' lined with Tyr398 (3.43 Å), Tyr435 (5.12 Å), and FAD. Phe343 (3.38 Å), Gln206 (3.80 Å), Ile199 (2.26 Å), Try326 (3.80 Å), and Ile316 (4.24 Å) are the surrounding residues of pyrazole ring. The better binding mode of **5i** with MAO-A explains the observation of the slightly higher MAO-A inhibitory potency of this compound.

Figure 8a shows the binding modes of compound **5l** into the MAO-A binding cavity. Analysis of the docking results of compound **5l** complexed with MAO-A reveals that its 4(3*H*)-quinazolinone ring was oriented among Tyr407 (2.49 Å), Phe352 (3.05 Å), side chains, and FAD (2.72 Å). The hydroxyl moiety of Glu216 and N1 nitrogen of the pyrazole ring is also in close proximity (2.88 Å). Ser209 (2.92 Å), Cys323 (3.15 Å), and Ile335 (3.41 Å) are the other favorable interactions stabilizing **5l** in the MAO-A cavity.

The binding mode of inhibitor **5l** within the MAO-B cavity is shown in Figure 8b. Contrary to most of the docking modes, the 4(3*H*)-quinazolinone moiety was not stacked between Tyr 398 and Tyr435. The aromatic ring of 4(3*H*)-quinazolinone is vertically oriented away from these two side chains and is much closer to the Tyr398 side chain (3.10 Å) than Tyr435 (5.13 Å). It was seen that the Gln206 (3.98 Å), Ile199 (2.17 Å) are the other important interactions with **5l**. The better binding mode of **5l** with MAO-A explains the observation of the much higher MAO-A inhibitory potency of this compound than that of MAO-B.

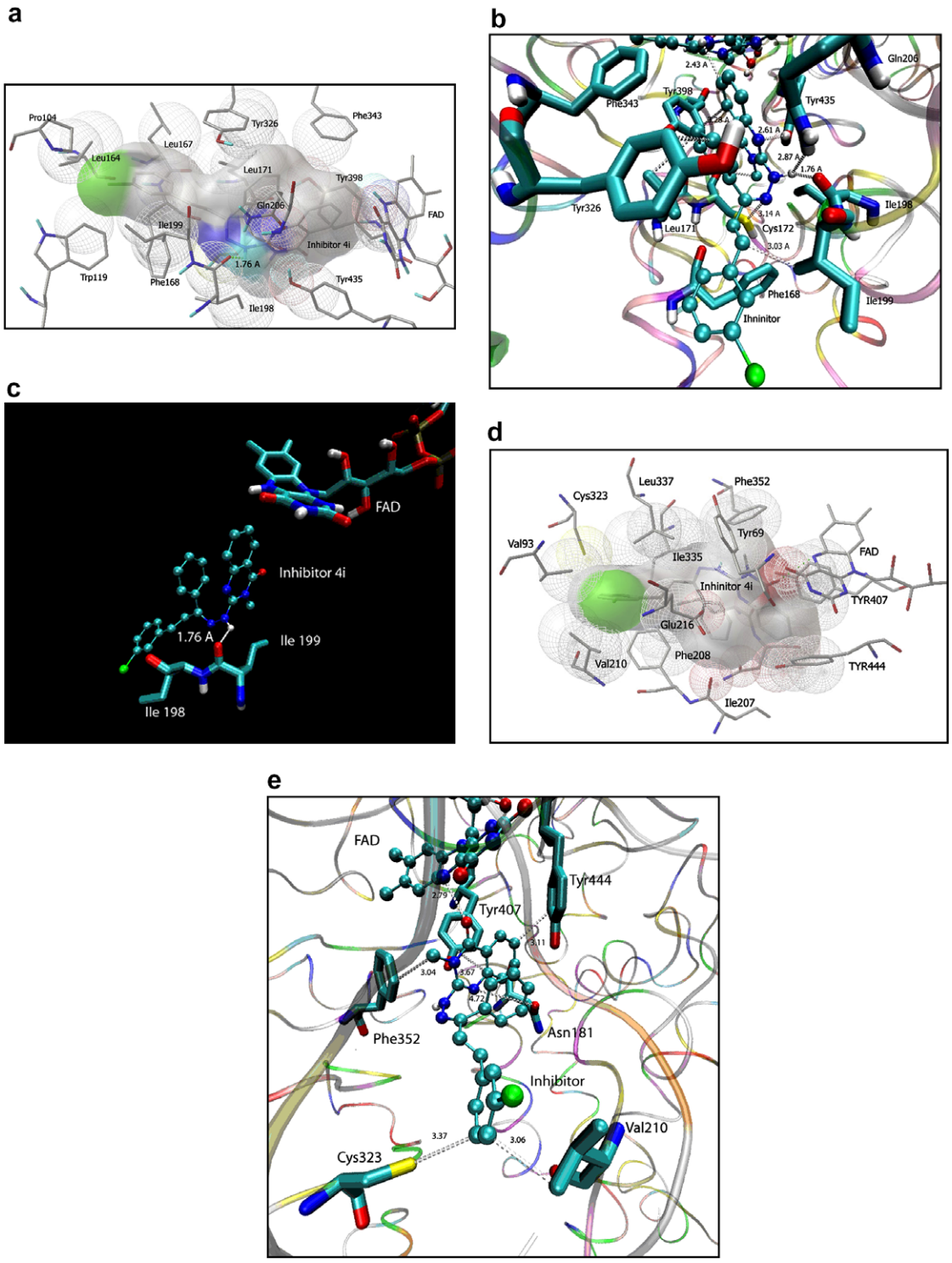

Figure 4. (a) Compound **4i** in the active site- of MAO-B. The shaded volume shows the van der Waals volume of the inhibitor **4i**. The hydrogen bond distance was indicated as 1.76 Å. Figure was generated by Using AutoDock Tools 1.5.1 (Ref. 68). (b) Binding model of **4i** in MAO-B active site. (c) Inhibitor **4i** in the active site of MAO-B. Here, only the hydrogen bonding residues were shown for clearness. (d) Compound **4i** in the active site of MAO-A. The shaded volume shows the van der Waals volume of the inhibitor **41**. Figure was generated by using AutoDock Tools 1.5.1 (Ref. 68). (e) Binding model of **4i** in MAO-1A active site.

2.5. Pharmacology

Due to the lipophilic character of the compounds, pharmacological activity tests were directed to assess the various effects of these compounds on the central nervous system. The effects of the compounds on anxiety and depression were evaluated by Porsolt's forced swimming test[44] and plus-maze,[45] respectively (Table 4).

Although the use of monoamine oxidase inhibitors (MAOIs) for patients with depressive disorders is well established,[46,47] most of the newly synthesized compounds (**4a, 4c–4f, and 5a–5f**) which carry furyl, thienyl group on C-5 did not show a marked antidepressant activity in Porsolt's forced swimming test in contrast to previously synthesized compounds carrying phenyl groups at C-5 of the 2-pyrazoline ring where the activity observed may be mainly

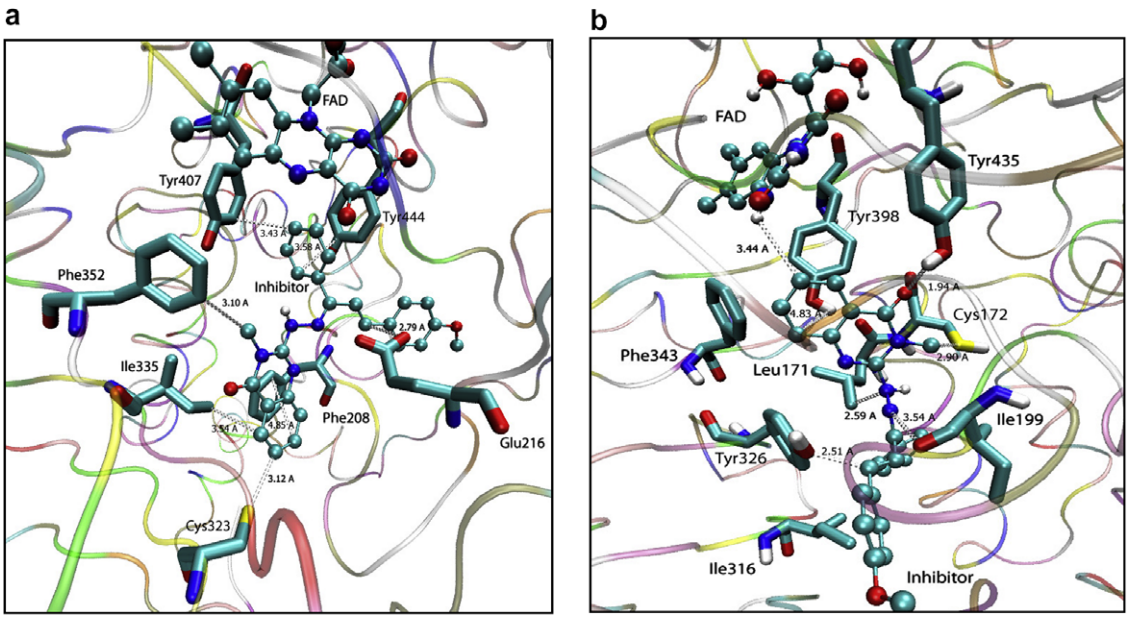

Figure 5. (a) Binding model of **4k** in MAO-A active site. (b) Binding model of **4k** in MAO-B active site.

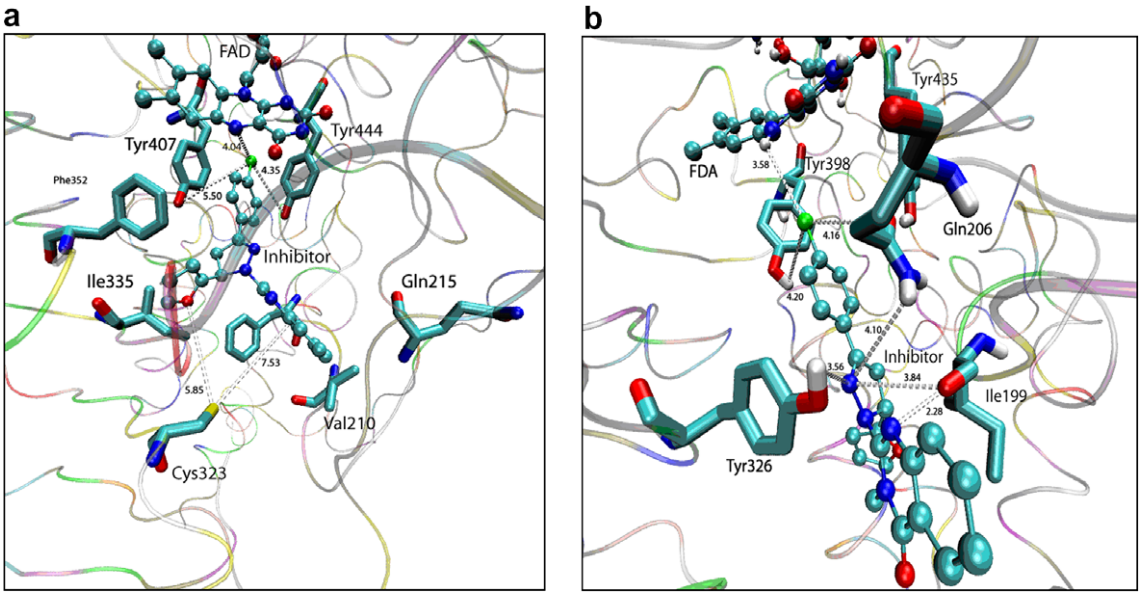

Figure 6. (a) Binding model of **5e** in MAO-A active site. (b) Binding model of **5e** in MAO-B active site.

based on the substituent effect (**4b, 4g, 4i, 4j, 4k, 4l**, and **5g–5l**). These active compounds decreased the duration of immobility. The activities of **5g** and **5i** are more than that of moclobemide; the others are as active as moclobemide.

In this study the use of furyl and thienyl rings instead of phenyl moiety gives us the opportunity to discuss the ring effect which brings about sterical and electronic differences in the molecules and it seems that these rings do not contribute to antidepressant activity. But this result may also be related to the test method used. The application of the modified behavioral despair test method[48] is our future aim in order to confirm these results.

Although there is evidence of a direct relationship between the plasma concentration of MAO and the antidepressant response of MAOIs[49,50] a precise mechanism underlying the anxiolytic effects of MAOIs has not been well defined. Nevertheless we applied the plus-maze test to get additional evidence for the elevation level of cathechol amines by the synthesized compounds. The experimental data have shown that most of the new and previously synthesized compounds possessed no anxiolytic activity except **4b, 4g**, **4n, 5a, 5d, 5h, and 5j. Because these compounds** (**4b, 4g, 4n, 5a, 5d, 5h, and 5j**) decreased the time spent in the closed arm. But **5b** seems an anxiogenic agent because of the decrease of the number of the entries and insignificant increase of the time spent in the closed arm.

Despite the clinical efficacy of MAOIs in some anxiety disorders,[51] it was reported that that these compounds do not usually show anxiolytic-like effects in experimental models of anxiety.[52,53] However, it was also reported that the MAOIs such as befloxatone and moclobemide exhibited anxiolytic-like effects in the elevated plus-maze in rats and the light/dark choice test

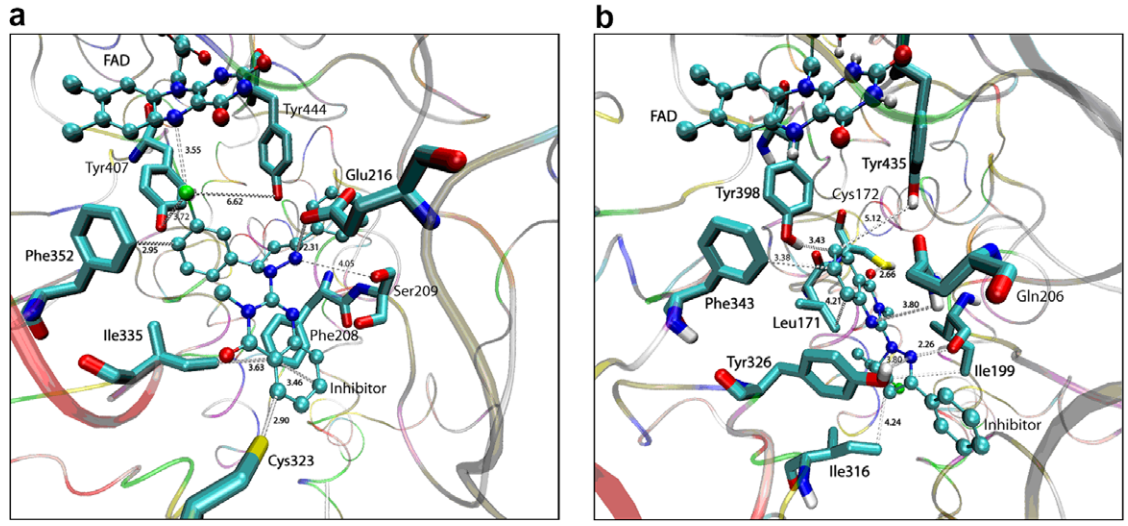

Figure 7. (a) Binding model of **5i** in MAO-A active site. (b) Binding model of **5i** in MAO-B active site.

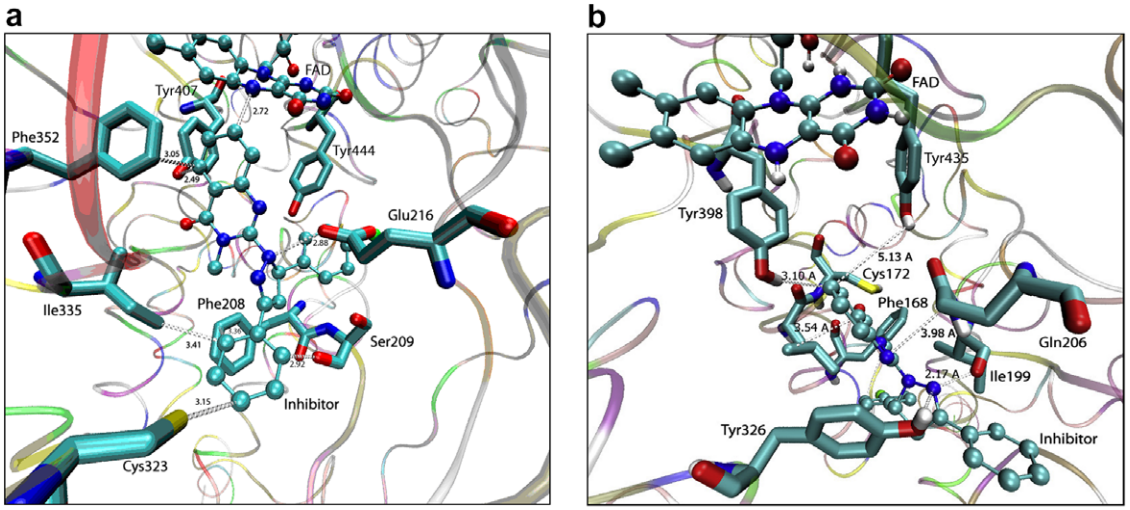

Figure 8. (a) Binding model of **5l** in MAO-A active site. (b) Binding model of **5l** in MAO-B active site.

in mice.[54,55] The reasons for this inconsistency on drug effects are not yet clear since it has been suggested that classical animal models of anxiety are insensitive to the action of these compounds.[55]

3. Conclusion

It is worth noting that the main difference in the MAO-inhibitory activities of pyrazole type compounds **5a–5l** was found when the 5-membered heterocycle on the pyrazole ring is replaced by a 6-membered heterocycle. This replacement appeared to be responsible for the remarkable differences in the inhibition activity mainly against MAO-A/MAO-B isoforms, respectively. Compounds **5a–5f** bearing a 5-membered ring at 5 the position showed MAO-B inhibition while compounds **5g–5l** carrying a 6-membered ring at the same position were inhibiting MAO-A. From a careful examination of the reported data, it can be emphasized that some substituents, in particular of the 3- and 5-phenyl groups, have a strong influence on A-selectivity.

The comparison of in vitro and in vivo test results shows that previously synthesized compounds (**4g, 4i–4l, and 5g–5l**) seem to be active in the applied pharmacological activity tests in parallel to MAO-A inhibition. The lack of in vivo activity of compounds **4a–4f**/**5a–5f** might be related to their MAO-B inhibition. As a result these new synthetic compounds proved to be reversible, potent, and selective inhibitors of monoamine oxidase-B rather than of monoamine oxidase-A, and are promising candidates to further advance drug discovery efforts.

The results obtained in the monoamine oxidase inhibitory study show that compound **4i** is able to differentially inhibit MAO-B, in preference to MAO-A, a behavior that can be rationalized on the basis of the structural differences of MAO-B and MAO-A active sites. The binding pose resulting from the docking studies of these compounds revealed the detailed structural information between the active site residues and the inhibitors. Nevertheless, many experimental studies have shown that MAOs isolated from different sources/species (rat, human or mouse liver, etc.) exhibit different binding modes to the MAO inhibitors possibly resulting from the differences in the volume and shape of the active sites of the

Table 4
Antidepressant and anxiolytic activities of newly synthesized compound

Compound[a]	*n*	Anxiolytic activity		Antidepressant activity
		Time spent in the closed arm ± SD[a]	Number of the entries[b] *X* ± SD	Duration of immobility (s) mean ± SD[c]
4a	7	204.71 ± 55.09	5.57 ± 2.94	65.57 ± 15.90
4b	7	162.17 ± 36.83*	8.50 ± 2.26	50.39 ± 12.90*
4c	7	206.29 ± 23.51	8.00 ± 2.31	49.29 ± 11.71
4d	7	238.67 ± 20.85	5.14 ± 1.95	82.43 ± 29.44
4e	7	219.50 ± 15.73	6.75 ± 1.83	67.88 ± 12.12
4f	7	237.25 ± 17.45	4.63 ± 1.60	80.38 ± 20.69
5a	7	188.14 ± 31.61*	5.14 ± 2.61	74.14 ± 32.62
5b	7	244.50 ± 62.75	2.29 ± 1.11*	61.83 ± 22.82
5c	7	248.50 ± 12.64	5.13 ± 1.64	61.13 ± 16.56
5d	7	208.57 ± 20.60*	9.00 ± 0.82*	64.00 ± 28.31
5e	7	204.00 ± 39.80	4.86 ± 2.27	74.00 ± 27.57
5f	7	226.00 ± 29.39	5.57 ± 2.76	69.00 ± 15.98
Control (DMSO/water 1:4)	7	228.63 ± 11.55	6.25 ± 2.05	67.75 ± 9.75
4g	8	191.00 ± 49.39*	5.37 ± 2.56*	55.43 ± 21.55*
4h	8	284.20 ± 38.08	2.51 ± 1.52	125.86 ± 38.65
4i	8	246.87 ± 31.81	3.15 ± 1.55	54.57 ± 22.58*
4j	8	216.12 ± 47.69	6.37 ± 2.93*	79.25 ± 30.18*
4k	8	225.38 ± 51.50	4.50 ± 3.67	86.75 ± 25.77*
4l	8	218.71 ± 45.97	3.87 ± 1.73	65.57 ± 12.51*
4m	8	218.88 ± 35.83	5.75 ± 2.18*	90.23 ± 26.58
4n	8	209.63 ± 45.98*	5.63 ± 1.19*	130.57 ± 56.63
5g	8	222.27 ± 38.58	4.37 ± 1.84	27.00 ± 22.12**
5h	8	154.75 ± 76.5*	4.12 ± 2.69	42.37 ± 17.58*
5i	8	218.25 ± 93.51	3.75 ± 2.37	26.25 ± 19.12**
5j	8	178.25 ± 82.77*	3.87 ± 1.72	43.25 ± 26.54*
5k	8	162.43 ± 35.72	5.37 ± 2.58*	58.00 ± 25.10*
5l	8	230.00 ± 46.83	3.25 ± 1.90	65.12 ± 30.78*
Control (DMSO/water 1:4)	8	254.15 ± 31.77	3.00 ± 1.41	122.00 ± 37.84
Moclobemide (5 mg/kg)	7	250.72 ± 17.20	6.15 ± 2.15	54.30 ± 9.73*

[a] The amount of time spent in closed arms is decreased in anxiolytic agents and decreased in anxiogenic agents.
[b] The number of entries is increased in anxiolytic agents and is decreased in anxiogenic agents.
[c] The reduction time of immobility time in the FST is an established way to evaluate effectiveness of potential antidepressant drugs.
* $p < 0.05$.
** $p < 0.01$.

MAOs isolated.[14] Thus, further docking studies with the different models are needed. We think that the experimental data herein should be the most reliable unless these models were to be fully described. However, compound **4i** may be considered a promising lead in the treatment of Parkinson's disease and worth testing in future.

Overall, the results of this work will be useful in the rational design of novel selective and potent MAO inhibitors.

4. Experimental

4.1. Chemistry

All chemicals were obtained from Aldrich Chemical Co. (Steinheim, Germany). Melting points were determined through a Thomas Hoover capillary melting point apparatus and are uncorrected. Infrared (IR) spectra were obtained with a Bruker Vector 22 IR (Opus Spectroscopic Software Version 2.0) spectrometer using potassium bromide plates and the results were expressed in wave number (cm^{-1}). ^1H Nuclear magnetic resonance spectra were scanned on a Bruker 400 MHz UltraShield spectrometer or Bruker AC 80 MHz NMR instrument using chloroform ($CDCl_3$) as solvent. Chemical shifts are expressed in δ (parts per million) relative to tetramethylsilane. Splitting patterns are as follows: s, singlet; d, doublet; m, multiplet; b, broad; dd (doublet in doublet). The mass spectra were obtained with electron impact technique using a Direct Insertion Probe and Agilent 5973-Network Mass Selective Dedector at 70 eV. Elemental analyses (C, H, N) were performed on Leco CHNS 932 analyzer. The elemental analysis results for C, H, N were in the range of ±0.4% of the theoretical value for compounds **5a**–**5f**.

4.1.1. Synthesis of 3-methyl-2(1*H*)-thioxo-4(3*H*)-quinazolinone (2)

3-Methyl-2(1*H*)-thioxo-4(3*H*)-quinazolinone was synthesized as a result of the reaction of anthranilic acid with methyl isothiocyanate according to the method reported earlier (mp 261 °C).[56]

4.1.2. 2-Hydrazino-3-methyl-4(3*H*)-quinazolinone (3)

2-Hydrazino-3-methyl-4(3*H*)-quinazolinone was synthesized by refluxing of 3-methyl-2(1*H*)-thioxo-4(3*H*)-quinazolinone and hydrazine hydrate in 2-propanol for 4 h as published before (mp 256 °C).[57]

4.1.3. Preparation of 1,3-diphenyl-2-propen-1-ones (chalcones) (general procedure)

Chalcone derivatives were synthesized by condensing acetophenone or 4-substituted acetophenones with thiophen aldehyde or furfural previously according to the methods given.[58]

4.1.4. 2-(1′-Substituted phenyl-3′-heteroaryl-2′-propenylidene) hydrazine-3-methyl-4(3*H*)-quinazolinone derivatives (4)

A mixture of chalcones (0.01 mol) and 2-hydrazino-3-methyl-4(3*H*)-quinazolinone (0.01) and 2 mL of acetic acid in *n*-propanol (100 mL) was stirred under reflux for 4–7 h. After the reaction was cooled to room temperature, the resulting residue was filtered, washed with *n*-propanol and dried. Recrystallization of the crude product from ethanol gave **4** as a yellow solid.

4.1.4.1. 2-[1′-(4-Methylphenyl)-3′-thienyl-2′-propenylidene] hydrazine-3-methyl-4(3*H*)-quinazolinone (4a). 51%; mp 223 (chloroform–methanol); IR (KBr): 3366 (NH), 1678 (C=O),

1603 (C=C), 1495 cm^{-1} (C=N); ^1H NMR δ (ppm): 2.2 (3H, s, Ph–CH_3), 3.6 (3H, s, N–CH_3), 6.6 (1H, d, *J* = 13 Hz, 2′-CH), 7.85 (1H, d, *J* = 13 Hz, 3′-CH), 6.9–8.2 (13H, m, Arom-H); MS (70 eV, EI): 400 (M+), 291 (100%), 284, 283, 119. Calculated for $C_{23}H_{20}N_4OS$ (400.50): C, 68.98; H, 5.03; N, 13.99. Found: C, 68.72; H, 4.85; N, 13.77.

4.1.4.2. 2-[1′-(4-Chlorophenyl)-3′-thienyl-2′-propenylidene]hydrazine-3-methyl)-4(3*H*)-quinazolinone (4b). 79%; mp 210 (chloroform–methanol); IR (KBr): 3366 (NH), 1679 (C=O),1604 (C=C), 1492 cm^{-1} (C=N); ^1H NMR δ (80 MHz) (ppm): 3.6 (3H, s, N–CH_3), 6.9–8.2 (13H, m, Arom-H); MS (70 eV, EI): 422 (M^++2), 420 (M^+), 283, 197 (100%), 159, 119. Calculated for $C_{22}H_{17}ClN_4OS$ (420.92): C,62.78; H,4.07; N,13.31. Found: C, 62.92; H, 4.32; N, 13.11 .

4.1.4.3. 2-[1′-(4-Methoxyphenyl)-3′-thienyl-2′-propenylidene] hydrazine-3-methyl-4(3*H*)-quinazolinone (4c). 55%; mp 188 (chloroform–methanol); IR (KBr): 3342 (NH), 1684 (C=O), 1586 (C=C), 1503 cm^{-1} (C=N); ^1H NMR δ (ppm): 3.84 (3H, s, N–CH_3), 3.89 (3H, s, Ph–OCH_3), 7 (1H, d, *J* = 16 Hz, 2′-CH), 7.6 (1H, d, *J* = 16 Hz, 3′-CH), 6.9–8.2 (11H, m, Arom-H); MS (70 eV, EI): 416 (M^+,100%), 283, 159, 119. Calculated for $C_{23}H_{20}N_4O_2S$ (416.50): C, 66.33; H, 4.84; N, 13.45. Found: C, 66.46; H, 5.24; N, 13.22.

4.1.4.4. 2-[1′-(4-Methylphenyl)-3′-furyl-2′-propenylidene]hydrazine-3-methyl-4(3*H*)-quinazolinone (4d). 56%; mp 199 (chloroform–methanol); IR (KBr): 3257 (NH), 1678 (C=O),1584 (C=C), 1486 cm^{-1} (C=N); ^1H NMR δ (ppm): 2.4 (3H, s, Ph–CH_3), 3,6 (3H, s, N–CH_3), 6.7 (1H, d, *J* = 16 Hz, 2′-CH), 7.9 (1H, d, *J* = 16 Hz, 3′-CH), 6.4–8.2 (11H, m, Arom-H); MS (70 eV, EI): 384 (M+), 291, 192 (100%), 159, 119. Calculated for $C_{23}H_{20}N_4O_2$ (384.44): C, 71.86; H, 5.24; N, 14.57. Found: C, 72.05; H, 5.44; N, 14.34.

4.1.4.5. 2-[1′-(4-Chlorophenyl)-3′-furyl-2′-propenylidene]hydrazine-3-methyl)-4(3*H*)-quinazolinone (4e). 64%; mp 190 (chloroform–methanol); IR (KBr): 3325 (NH), 1677 (C=O), 1608 (C=C), 1489 cm^{-1} (C=N); ^1H NMR δ (ppm): 3.8 (3H, s, N–CH_3), 6.8 (1H, d, *J* = 14 Hz, 2′-CH), 7.2–8.5 (10H, m, 3′-CH, Arom-H).; MS (70 eV, EI): 406 (M+2), 404, 267, 252 (100%), 159, 119. Calculated for $C_{22}H_{17}ClN_4O_2$ (404.86): C, 65.27; H, 4.23; N, 13.84. Found: C, 65.43; H, 4.32; N, 14.10.

4.1.4.6. 2-[1′-(4-Methoxyphenyl)-3′-furyl-2′-propenylidene]hydrazine-3-methyl-4(3*H*)-quinazolinone (4f). 72%; mp 178 (chloroform–methanol); IR (KBr): 3337 (NH), 1670 (C=O), 1586 (C=C), 1505 (C=N); ^1H NMR δ (ppm): 3.6 (3H, s, N–CH_3), 3.87 (3H,s, Ph–OCH_3), 6.7 (1H, d, *J* = 14 Hz, 2′-CH), 7.9 (1H, d, *J* = 14 Hz, 3′-CH), 6.4–8.1 (11H, m, Arom-H), 9.4 (1H, br s, NH); MS (70 eV, EI): 400 (M^+), 225 (100%), 169, 119. Calculated for $C_{23}H_{20}N_4O_3$ (400.44): C, 68.99; H, 5.03; N, 13.99. Found: C, 68.86; H, 4.86; N, 13.98.

4.1.4.7. 2-(1,3′-Diphenyl-2′-propenylidene)hydrazine-3-methyl -4(3*H*)-quinazolinone (4g). 40%; mp 173, $C_{24}H_{20}N_4O$; Ref. 59.

4.1.4.8. 2-[1′-Phenyl-3′-(4-chlorophenyl)-2′-propenylidene]hydrazine-3-methyl-4(3*H*)-quinazolinone (4h). 60%; mp 153, $C_{24}H_{19}N_4OCl$; Ref. 59.

4.1.4.9. 2-[1′-Phenyl-3′-(3-chlorophenyl)-2′-propenylidene]hydrazine-3-methyl-4(3H)-quinazolinone (4i). 46%; mp 175, $C_{24}H_{19}N_4OCl$; Ref. 59.

4.1.4.10. 2-[1′-Phenyl-3′-(4-methylphenyl)-2′-propenylidene] hydrazine-3-methyl)-4(3*H*)-quinazolinone (4j). 91%; mp 181, $C_{24}H_{19}N_4OBr$; Ref. 59.

4.1.4.11. 2-[1′-Phenyl-3′-(4-methoxyphenyl)-2′-propenylidene] hydrazine-3-methyl-4(3*H*)-quinazolinone (4k). 65%; mp 160, $C_{25}H_{22}N_4O$; Ref. 59.

4.1.4.12. 2-[1′-Phenyl-3′-(4-bromophenyl)-2′-propenylidene] hydrazine-3-methyl)-4(3*H*)-quinazolinone (4l). 61%; mp 217, $C_{25}H_{22}N_4O_2$; Ref. 59.

4.1.4.13. 2-[1′-Phenyl-3′-(4-ethoxyphenyl)-2′-propenylidene] hydrazine-3-methyl-4(3*H*)-quinazolinone (4m). 50%; mp 180, $C_{26}H_{24}N_4O_3$; Ref. 59.

4.1.4.14. 2-[1′-Phenyl-3′-(3,4-dimethoxyphenyl)-2′-propenylidene]hydrazine-3-methyl-4(3*H*)-quinazolinone (4n). 47%; mp 170, $C_{26}H_{24}N_4O_3$; Ref. 59.

4.1.5. 2-(3-Substituted phenyl-5′-heteroaryl-2′-pyrazoline-1-yl) -3-methyl-4(3*H*)-quinazolinone derivatives (5)

A solution of 2-(1′-substituted phenyl-3′-heteroaryl-2′-propenylidene)hydrazine-3-methyl-4(3*H*)-quinazolinones **4** (0.01 mol) in glacial acetic acid was stirred under reflux for 72 h. The resulting solution was poured into ice-water, neutralized with concentrated NaOH solution, and extracted with ethyl acetate. The organic phase was dried over magnesium sulfate, filtered, and evaporated to dryness to yield the oily residue. The crude product was further purified by chromatography on a silica gel column (elution with chloroform) followed by crystallization from diethyl ether to give **5** as a white solid.

4.1.5.1. 2-[(3-(4-Methylphenyl)-5′-thienyl-2′-pyrazoline-1-yl]-3-methyl-4(3*H*)-quinazolinone (5a). 94%; mp 201 (chloroform–methanol); IR (KBr): 1671 (C=O), 1563 (C=C), 1474 (C=N); ^1H NMR δ (ppm): 2.7 (3H, s, Ph–CH_3), 3.6 (1H, t, H_A), 4.05 (4H, m, H_B and N–CH_3), 6.5 (1H, t, H_X), 7.2–8.5 (11H, m, Arom-H); MS (70 eV, EI): 400, 282, 268 (100%), 250. Calculated for $C_{23}H_{20}N_4OS$ (400.50): C, 68.98; H, 5.03; N, 13.99. Found: C, 68.86; H, 4.86; N, 13.98.

4.1.5.2. 2-[(3-(4-Chlorophenyl)-5′-thienyl-2′-pyrazoline-1-yl]-3-methyl-4(3*H*)-quinazolinone (5b). 93%; mp 191 (chloroform–methanol); IR (KBr): 1671 (C=O), 1563 (C=C), 1473 (C=N); ^1H NMR δ (80 MHz) (ppm): 3.4 (1H, s, H_A), 3.6 (1H, s, H_B), 3.8 (1H, s, N–CH_3), 6.5 (1H, m, H_X), 7.1–8.4 (11H, m, Arom-H); MS (70 eV, EI): 422 (M^++2), 420 (M^+), 282, 268 (100%), 250. Calculated for $C_{22}H_{17}ClN_4OS$ (420.92): C, 62.78; H, 4.07; N, 13.31. Found: C, 62.50; H, 3.73; N, 13.26 .

4.1.5.3. 2-[(3-(4-Methoxyphenyl)-5′-thienyl-2′-pyrazoline-1-yl]-3-methyl-4(3*H*)-quinazolinone (5c). 86%; mp 100 (chloroform–methanol); IR (KBr): 1669 (C=O), 1593 (C=C), 1471 (C=N); ^1H NMR δ (ppm): 3.4 (1H, t, H_A), 3.8 (1H, m, H_B and N–CH_3), 3.9 (3H, s, Ph–OCH_3), 6.2 (1H, t, H_X), 6.94–8.22 (11H, m, Arom-H); MS (70 eV, EI): 416 (M^+), 418:(M+2), 282, 268 (100%), 250. Calculated for $C_{23}H_{20}N_4O_2S$ (416.50): C, 66.33; H, 4.84; N, 13.45. Found: C, 66.33; H, 5.73; N, 13.10.

4.1.5.4. 2-[(3-(4-Methylphenyl)-5′-furyl-2′-pyrazoline-1-yl]-3-methyl-4(3*H*)-quinazolinone (5d). 83%; mp 151 (chloroform–methanol); IR (KBr): 1672 (C=O), 1561 (C=C), 1474 (C=N); ^1H NMR δ (80 MHz) (ppm): 2.3 (3H, s, Ph–CH_3), 3.3 (1H, s, H_A), 3.4 (1H, s, H_B), 3.60 (3H, s, N–CH_3), 6 (1H, m, H_X), 6.8–8.1 (11H, m, Arom-H); MS (70 eV, EI): 384 (M+), 252 (100%), 119. Calculated for $C_{23}H_{20}N_4O_2$ (384.44): C, 71.86; H, 5.24; N, 14.57. Found: C, 72.20; H, 5.72; N, 14.46.

4.1.5.5. 2-[(3-(4-Chlorophenyl)-5′-furyl-2′-pyrazoline-1-yl]-3-methyl-4(3*H*)-quinazolinone (5e). 98%; mp 195 (chloro-

form–methanol); IR (KBr): 1671 (C=O), 1563 (C=C), 1472 (C=N); ^{1}H NMR δ (ppm): 3.4 (1H, t, H_A), 3.8 (4H, m, H_B and N–CH_3), 6.4 (1H, t, H_X), 7.0–8.1 (11H, m, Arom-H) 406 (M+2), 404 (M^+), 268, 252 (100%), 215, 119; MS (70 eV, EI): 406 (M+2), 404 (M^+), 268, 252 (100%), 215, 119. Calculated for $C_{22}H_{17}ClN_4O_2$ (404.86): C, 65.27; H, 4.23; N, 13.84. Found: C, 64.89; H, 4.19; N, 13.47.

4.1.5.6. 2-[(3-(4-Methoxyphenyl)-5′-furyl-2′-pyrazoline-1-yl]-3-methyl-4(3*H*)-quinazolinone (5f). 85%; mp 168 (chloroform–methanol); IR (KBr): 1686 (C=O), 1596 (C=C), 1471 (C=N); ^{1}H NMR δ (ppm): 3.4 (1H, s, H_A), 3.7 (1H, s, H_B), 3.76 (3H, s, N–CH_3), 3.84 (3H, s, Ph–OCH_3), 6.1 (1H, t, H_X), 6.3–8.2 (11H, m, Arom-H); MS (70 eV, EI): 400 (M^+), 267, 252 (100%). Calculated for $C_{23}H_{20}N_4O_3$ (400.44): C, 68.99; H, 5.03; N, 13.99. Found: C, 68.86; H, 4.86; N, 13.98.

4.1.5.7. 2-(3,5′-Diphenyl-2′-pyrazoline-1-yl)-3-methyl-4(3*H*)-quinazolinone (5g). 59%; mp 165, $C_{24}H_{20}N_4O$; Ref. 59.

4.1.5.8. 2-[(3-Phenyl-5′-(4-chlorophenyl)-2′-pyrazoline-1-yl]-3-methyl-4(3*H*)-quinazolinone (5h). 79%; mp 125, $C_{24}H_{19}N_4OCl$; Ref. 59.

4.1.5.9. 2-[(3-Phenyl-5′-(3-chlorophenyl)-2′-pyrazoline-1-yl]-3-methyl-4(3*H*)-quinazolinone (5i). 99%; mp 149, $C_{24}H_{19}N_4OCl$; Ref. 59.

4.1.5.10. 2-[(3-Phenyl-5′-(4-methylphenyl)-2′-pyrazoline-1-yl]-3-methyl)-4(3*H*)-quinazolinone (5j). 98%; mp 170, $C_{26}H_{24}N_4OBr$; Ref. 59.

4.1.5.11. 2-[(3-Phenyl-5′-(4-methoxyphenyl)-2′-pyrazoline-1-yl]-3-methyl-4(3*H*)-quinazolinone (5k). 81%; mp 120, $C_{25}H_{22}N_4O$; Ref. 59.

4.1.5.12. 2-[(3-Phenyl-5′-(4-bromophenyl)-2′-pyrazoline-1-yl]-3-methyl-4(3*H*)-quinazolinone (5l). 66%; mp 140, $C_{25}H_{22}N_4O_2$; Ref. 59.

4.2. Single crystal X-ray crystallographic data of 5a

The data collection was performed on a CAD-4 diffractometer employing graphite-monochromated CuKα radiation (λ = 1.54184 Å). Crystallographic and refinement parameters are summarized in Table 1. Three standard reflections were measured every 2 h. The structure was solved by direct methods. The refinement was made with anisotropic temperature factors for all nonhydrogen atoms. The hydrogen atoms were generated geometrically. An empirical Ψ scan absorption correction was applied. Some selected bond lengths, angles and torsion angles are listed in Figure 2.

Crystallographic data (excluding structure factors) for compound **5a** reported in this paper have been deposited with the Cambridge Crystallographic Data Centre as supplementary publication number CCDC-690526. Copies of the data can be obtained, free of charge, on application to CCDC, 12 Union Road, Cambridge CB2 1EZ, UK (fax: +44 (0) 1223 336033 or e-mail: deposit@ccdc.cam.ac.uk).

4.3. Biochemistry

All chemicals used were purchased from Sigma–Aldrich Co. (Germany).

4.3.1. Isolation of MAO from rat liver homogenates

The Ethics Committee of Laboratory Animals at Hacettepe University, Turkey (2001/25-4), approved the animal experimentation. MAO was purified from the rat liver according to the method of Holt with some modifications.[60] Liver tissue was homogenized 1:40 (w/v) in 0.3 M sucrose. Following centrifugation at 1000g for 10 min, the supernatant was centrifuged at 10,000g for 30 min to obtain crude mitochondrial pellet.

The pellet was incubated with CHAPS of 1% at 37 °C for 60 min. and centrifuged at 1000g for 15 min. Pellet was resuspended in 0.3 M sucrose and was layered onto 1.2 M sucrose, centrifuged at 53,000g for 2 h and resuspended in potassium phosphate buffer, pH 7.4, kept at −70 °C until used.

4.3.2. Measurement of MAO activity

Total MAO activity was measured spectrophotometrically according to the method of Holt.[60] The assay mixture contained a chromogenic solution consisted of 1 mM vanillic acid, 500 μM 4-aminoantipyrine, and 4 U mL^{-1} peroxidase type II in 0.2 M potassium phosphate buffer, pH 7.6. The assay mixture contained 167 μl chromogenic solution, 667 μl substrate solution (500 μM *p*-tyramine), and 133 μl potassium phosphate buffer, pH 7.6. The mixture was preincubated at 37 °C for 10 min before the addition of enzyme. Reaction was initiated by adding the homogenate (100 μl), and increase in absorbance was monitored at 498 nm at 37 °C for 60 min. The molar absorption coefficient of 4654 M^{-1} cm^{-1} was used to calculate the initial velocity of the reaction. The results were expressed as nmol h^{-1} mg^{-1}.

4.3.3. Selective measurement of MAO-A and MAO-B activities

Homogenates were incubated with the substrate *p*-tyramine (500 μM to measure MAO-A and 2.5 mM to measure MAO-B) following the inhibition of one of the MAO isoforms with selective inhibitors. Aqueous solutions of clorgyline or pargyline (50 μM), as selective MAO-A and -B inhibitor, were added to homogenates at the ratio of 1:100 (v/v), yielding the final inhibitor concentrations of 0.50 μM. Homogenates were incubated with these inhibitors at 37 °C for 60 min prior to activity measurement. After incubation of homogenates with selective inhibitors, total MAO activity was determined by the method described above.

4.3.4. Analysis of the kinetic data

Newly synthesized compounds were dissolved in dimethyl sulfoxide (DMSO), maximum concentration 1% and used in the concentration range of 1–1000 μM. Inhibitors were incubated with the purified MAO at 37 °C for 0, 10, 20, 40, and 60 min prior to adding to the assay mixture. Reversibility of the inhibition of the enzyme by novel compounds was assessed by dialysis performed over 24 h at 4 °C relative to a potassium phosphate buffer, pH 7.6, capable of restoring 98–100% of the enzyme activity.

Kinetic data for interaction of the enzyme with the compounds were determined using Microsoft Excel package program. The initial rates were obtained at five different substrate concentrations (50–500 μM) in the absence and presence of four different inhibitor concentrations. The slopes of the Lineweaver–Burk plots were plotted versus the inhibitor concentration and the K_i value was determined from the *x*-axis intercept as $-K_i$. Each K_i value is the representative of single determination where the correlation coefficient (R^2) of the replot of the slopes versus the inhibitor concentrations was at least 0.98.

IC_{50} values were determined from plots of residual activity percentage, calculated in relation to a sample of the enzyme treated under the same conditions without inhibitor, versus inhibitor concentration [I].

4.3.5. Protein determination

Protein was determined according to the method of Bradford,[61] in which bovine serum albumin was used as standard.

4.4. Molecular docking

4.4.1. Protein setup

The crystal structures human monoamine oxidase-A (PDB entry code: 2BXS, co-crystalized with the inhibitor clorgyline) and human monoamine oxidase-B (PDB entry code: 1S3E co-crystalized with the inhibitor 6-hydroxy-*N*-propargyl-1(*R*)-aminoindan) were obtained from the Protein Data Bank (http://www.rcsb.org).[62–65] Studies were carried out on only one subunit of the enzymes. The PDB files were edited and the β-chains were removed together with their irreversible inhibitors.

In order to relieve the crystal structure tension and to make the protein available to use in the AutoDock docking simulation program, all polar hydrogens were added with the GROMACS modeling package.[66,67] The obtained structure was optimized in 400 steps of conjugate gradient minimization, employing the GROMOS-87 force field. During minimization the heavy atoms were kept fixed at their initial crystal coordinates, but added hydrogens were made free to move. Minimization was performed under a vacuum medium.

The AutoDockTools (ADT),[68] graphical user interface, program was employed to setup the enzymes: all hydrogens were added, Gasteiger[69] charges were calculated and nonpolar hydrogens were merged to carbon atoms. For macromolecules, generated pdbqt files were saved.

4.4.2. Ligands

The 3D structures of ligand molecules were built, optimized (PM3) level, and saved in mol2 format with the aid of the molecular modeling program Spartan (Wavefunction Inc.).[70] These partial charges of Mol2 files were further modified by using the ADT package (version 1.4.6) so that the charges of the nonpolar hydrogens atoms assigned to the atom to which the hydrogen is attached. The resulting files were saved as pdbqt files.

4.4.3. Molecular docking

AutoDock 4.01,[71,72] was employed for all docking calculations. The AutoDockTools program was used to generate the docking input files. In all docking a grid box size of $80 \times 80 \times 80$ points in *x*, *y*, and *z* directions was built, and because the location of the inhibitor in the complex was known,[73,74] the maps were centered on N5 atom of the flavin (FAD) in the catalytic site of the protein. A grid spacing of 0.375 Å (approximately one forth of the length of carbon–carbon covalent bond) and a distances-dependent function of the dielectric constant were used for the calculation of the energetic map. Ten runs were generated by using Lamarckian genetic algorithm searches. Default settings were used with an initial population of 50 randomly placed individuals, a maximum number of 2.5×10^6 energy evaluations, and a maximum number of 2.7×10^4 generations. A mutation rate of 0.02 and a crossover rate of 0.8 were chosen. Results differing by less than 0.5 Å in positional root-mean-square deviation (RMSD) were clustered together and the results of the most favorable free energy of binding were selected as the resultant complex structures. All calculations were carried out on an Mac OS X machine of intel core duo processor at 2 GHz with 1 GB of RAM. The resultant structure files were analyzed using VMD[75] (Visual Molecular Dynamics) visualization programs.

4.5. Pharmacology

Local bred albino mice of either sex weighing 20–25 g were used in all experiments. They were housed eight per cage and kept in a room with controlled temperature (20 ± 2 °C) and 12 h light/dark cycle. All animals were allowed ad libitum access to food and water. All compounds were dissolved in DMSO/water (1:4) and injected to the animals intraperitoneally at 100 mg/kg doses in approximately 0.1 mL volume 1 h before the test. 0.1 mL DMSO/water (1:4) was given to the control animals. A plus-maze test was applied for anxiolitic activity of the compounds.[76]

Antidepressant activity was tested by Porsolt forced swimming test (behavioral despair test).[77] Each animal was used for the plus-maze at first and then for the forced swimming test. All experiments for animal testing were approved by Osman Gazi University School of Medicine Animal Use and Care Committee.

4.5.1. Elevated plus-maze test

The elevated plus-maze is used to determine the mouse's unconditioned response to a potentially dangerous environment and anxiety-related behavior is measured by the degree to which the mouse avoids the unenclosed arms of the maze. The test is particularly useful in testing the effects of anxiolytic and anxiogenic drugs.

It is a standard test of fear and anxiety in which the animal is placed in the center of an elevated 4-arm maze in which 2 arms are open 50×10 cm and 2 are enclosed $50 \times 10 \times 40$ cm with an open roof. The two open arms were opposite to each other. The maze was elevated to a height of 50 cm. The measures indicated in the procedure section were taken by two observers, sitting in the same room with the maze.

Mice were placed in the center of the maze and the following measures scored by two observers for 5 min. The number of times the animal enters each of the arms and the time spent in each arm is noted.[76] Two indices of anxiety are obtained: the amount of time spent in closed arms and the number of entries into the arms. The test is rapid and to be sensitive to the effects of both anxiolytic and anxiogenic agents, anxiolytic agents decreasing, and anxiogenic agents increasing the amount of time spent in closed arms; anxiolytic agents increasing and anxiogenic agents decreasing the number of entries.[78,79]

4.5.2. Forced swimming test

Individual mice were forced to swim vertical plexiglass cylinders (height: 25 cm, diameter 10 cm) containing 6 cm of water at 21–23 °C 1 h after a single ip injection. Mice were dropped into the cylinder and left there for 6 min. An observer counted the total amount of time that the mice spent immobile. Immobility was defined as 'floating motionless or making only those movements necessary to keep its head above the water'.[80] Because little immobility is observed during the first 2 min the total duration of immobility was measured during the last 4 min. The moused was judged to be immobile whenever it remained floating passively in the water in a slightly hunched but upright position, while its head was just above the surface.[77]

Statistical analysis results were expressed as means ± SD and evaluated by Student's *t* test.

Acknowledgment

This study was supported by the Hacettepe University Research Fund (Project No. 07 D03 301 003).

References and notes

1. Youdim, M. B. H.; Edmonson, D.; Tipton, K. F. *Nat. Rev. Neurosci.* **2006**, *7*, 295.
2. Coutts, R. T.; Baker, G. B.; Danielson, T. J. New Developments in Monoamine Oxidase Inhibitors. In *Developments of Drugs and Modern Medicines*; Gorrod, J. W., Gibson, G. G., Mitchard, M., Eds.; Part I. Drug Design; Ellis Horwood Ltd: Chichester, 1986; p 40.
3. Kalgutkar, A. S.; Castagnoli, N., Jr. *Med. Res. Rev.* **1995**, *15*, 325.
4. Johston, J. P. *Biochem. Pharmacol.* **1968**, *17*, 1285.
5. Knoll, J.; Magyar, K. *Adv. Biochem. Psychophys.* **1972**, *5*, 393.
6. O'Carroll, A.; Fowler, C. J.; Phillips, J. P.; Tobbia, I.; Tipton, K. F. N.-S. *Arch. Pharmacol.* **1983**, *322*, 198.
7. Rudorfer, M. V.; Potter, W. Z. *Drugs* **1989**, *37*, 713.

8. Pacher, P.; Kohegyi, E.; Keckemeti, V.; Furst, S. *Curr. Med. Chem.* **2001**, *8*, 89.
9. Pacher, P.; Keckemeti, V. *Curr. Med. Chem.* **2004**, *11*, 925.
10. Wouters, J. *Curr. Med. Chem.* **1998**, *5*, 137.
11. Carreiras, M. C.; Marco, J. L. *Curr. Pharm. Des.* **2004**, *10*, 367.
12. Binda, C.; Newton-Vinson, P.; Hubálek, F.; Edmondson, D. E.; Mattevi, A. *Nat. Struct. Biol.* **2002**, *9*, 22.
13. Edmondson, D. E.; Binda, C.; Mattevi, A. *Neurotoxicology* **2004**, *25*, 63.
14. De Colibus, L.; Li, M.; Binda, C.; Lustig, A.; Edmondson, D. E.; Mattevi, A. *Proc. Natl. Acad. Sci. U.S.A.* **2005**, *102*, 12684.
15. Hubálek, F.; Binda, C.; Khalil, A.; Li, M.; Mattevi, A.; Castagnoli, N.; Edmondson, D. E. *J. Biol. Chem.* **2005**, *280*, 15761.
16. Cesura, M. A.; Pletscher, A. *Prog. Drug Res.* **1992**, *38*, 171.
17. Tipton, K. F. *Biochem. J.* **1972**, *128*, 913.
18. Mc Kenna, K. F.; Baker, G. B.; Coutta, R. T. N.-S. *Arch. Pharmacol.* **1991**, *343*, 478.
19. Yamada, N.; Takahashi, S.; Todd, K. G.; Baker, G. B.; Paetsch, P. R. *J. Pharm. Sci.* **1993**, *82*, 934.
20. Parmar, S. S.; Pandey, B. R.; Dwivedi, C.; Harbison, R. D. *J. Pharm. Sci.* **1974**, *63*, 1152.
21. Soni, N.; Pande, K.; Kalsi, R.; Gupta, T. K.; Parmar, S. S.; Barthwal, J. P. *Res. Commun. Chem. Path.* **1987**, *56*, 129.
22. Manna, F.; Chimenti, F.; Bolasco, A.; Bizzarri, B.; Befani, O.; Pietrangeli, P.; Mondovi, B.; Turini, P. J. *Enzyme Inhib.* **1998**, *13*, 207.
23. Manna, F.; Chimenti, F.; Bolasco, A.; Secci, D.; Bizzarri, B.; Befani, O.; Turini, P.; Mondovi, B.; Alcaro, S.; Tafi, A. *Bioorg. Med. Chem. Lett.* **2002**, *12*, 3629.
24. Gökhan, N.; Yeşilada, A.; Uçar, G.; Erol, K.; Bilgin, A. A. *Arch. Pharm.* **2003**, *336*, 362.
25. Chimenti, F.; Bolasco, A.; Manna, F.; Secci, D.; Chimenti, P.; Befani, O.; Turini, P.; Giovannini, V.; Mondovi, B.; Cirilli, R.; La Torre, F. *J. Med. Chem.* **2004**, *47*, 2071.
26. Chimenti, F.; Maccioni, E.; Secci, D.; Bolasco, A.; Chimenti, P.; Granese, A.; Befani, O.; Turini, P.; Alcaro, S.; Ortuso, F.; Cirilli, R.; La Torre, F.; Cardia, M. C.; Distinto, S. *J. Med. Chem.* **2005**, *48*, 7113.
27. Gökhan Kelekçi, N.; Yabanoğlu, S.; Küpeli, E.; Salgın Gökşen, U.; Özgen, Ö.; Uçar, G.; Yeşilada, E.; Kendi, E.; Yeşilada, A.; Bilgin, A. A. *Bioorg. Med. Chem.* **2007**, *15*, 5775.
28. Yeşilada, A.; Gökhan, N.; Özer, İ.; Vural, K.; Erol, K. *Farmaco* **1996**, *51*, 775.
29. Uçar, G.; Gökhan, N.; Yeşilada, A.; Yabanoğlu, S.; Bilgin, A. A. *Hacettepe Univ. J. Fac. Pharm.* **2005**, *25*, 23.
30. Yabanoğlu, S.; Uçar, G.; Gökhan, N.; Salgın, U.; Yeşilada, A.; Bilgin, A. A. *J. Neural. Transm.* **2007**, *114*, 769.
31. Uçar, G.; Gökhan, N.; Yeşilada, A.; Bilgin, A. A. *Neurosci. Lett.* **2005**, *382*, 327.
32. Gupta, R. C.; Saxena, A. K.; Shanker, K.; Kishor, K. *Indian J. Pharm.* **1977**, *39*, 20.
33. Mısra, R. S.; Chaudhari, A.; Chaturvedi, A. K.; Parmar, S. S.; Sastry, V. R. *Pharmacol. Res. Commun.* **1977**, *9*, 437.
34. Srivastava, V. K.; Satsangi, R. K.; Kumar, P.; Kishor, K. *J. Physiol. Pharmacol.* **1980**, *24*, 361.
35. Lata, A.; Satsangi, R. K.; Srivastava, V. K.; Kishor, K. *Arzneimittel-Forsch.* **1982**, *32*, 24.
36. Shrimali, M.; Kalsi, R.; Dixit, K. S.; Barthwal, J. P. *Arzneimittel-Forsch.* **1991**, *41*, 514.
37. Sheldrick, G. M. SHELXL-97. Program for Crystal Structure Refinement, University of Göttingen, Germany, 1997.
38. Sheldrick, G. M. SHELXS-97. Program for Crystal Structure Solution, University of Göttingen, Germany, 1997.
39. North, A. C. T.; Phillips, D. C.; Mathews, F. S. *Acta Crystallogr.* **1968**, *A24*, 351.
40. Farrugia, L. J. *J. Appl. Crystallogr.* **1997**, *30*, 565.
41. Ozgen, O.; Koyunoglu, S.; Kendi, E.; Yesilada, A. *Struct. Chem.* **2005**, *16*, 61.
42. Krishna, R.; Velmurugan, D.; Shanmuga, S. M.; Raghunathan, R. *Acta Crystallogr.* **1999**, *C55*, 1676.
43. Isık, K.; Koysal, Y.; Ozdemir, Z.; Bilgin, A. A. *Acta Crystallogr.* **2006**, *E62*, o491.
44. Porsolt, R. D.; Anton, G.; Blavet, N.; Jalfre, M. *Eur. J. Pharmacol.* **1978**, *47*, 379.
45. Pellow, S.; Chopin, P.; File, S. E.; Briley, M. *J. Neurosci. Meth.* **1985**, *14*, 149.
46. Laux, G.; Volz, H. P.; Moller, H. J. *CNS Drugs* **1995**, *3*, 145.
47. Thase, M. E.; Trivedi, M. H.; Rush, A. J. *Neuropsychopharmacology* **1995**, *12*, 185.
48. Sunal, R.; Gümüşel, B.; Kayaalp, S. O. *Pharmacol. Biochem. Behav.* **1994**, *49*, 891.
49. Buller, R. *Clin. Neuropharmacol.* **1995**, *18*, S38.
50. Priest, R. G.; Gimbrett, R.; Roberts, W.; Steinert, J. *Acta Psychiat. Scand.* **1995**, *91*, 40.
51. Paslawski, T.; Treit, D.; Baker, G. B.; George, M.; Coutts, R. T. *Psychopharmacology* **1996**, *127*, 19.
52. Lecci, A.; Borsini, F.; Volterra, G.; Meli, A. *Psychopharmacology* **1990**, *101*, 255.
53. DeAngelis, L. *Biol. Psychiatry* **1997**, *42*, 14.
54. Caille, D.; Bergis, O. E.; Fankhauser, C.; Gardes, A.; Adam, R.; Charieras, T.; Grosset, A.; Rovei, V.; Jarreau, F. X. *J. Pharmacol. Exp. Ther.* **1996**, *277*, 265.
55. Griebel, G.; Perrault, G.; Sanger, D. J. *Psychopharmacology* **1997**, *131*, 180.
56. Butler, K.; Partridge, M. W. *J. Chem. Soc.* **1959**, 1512.
57. Fathalla, W.; Čajan, M.; Pazdera, P. *Molecules* **2001**, *6*, 557.
58. Mehra, H. S. *J. Indian Chem. Soc.* **1968**, *45*, 178.
59. Yeşilada, A.; Koyunuğlu, S.; Saygılı, N.; Küpeli, E.; Yeşilada, E.; Bedir, E.; Khan, I. *Arch. Pharm. Pharm. Med. Chem.* **2004**, *337*, 96.
60. Holt, A.; Sharman, D. F.; Baker, G. B.; Pelcic, M. M. *Anal. Biochem.* **1997**, *244*, 384.
61. Bradford, M. M. *Anal. Biochem.* **1976**, *72*, 248.
62. Binda, C.; Hubalek, F.; Li, M.; Edmondson, D. E.; Mattevi, A. *FEBS Lett.* **2004**, *564*, 225.
63. Binda, C.; Hubalek, F.; Li, M.; Herzig, Y.; Sterling, J.; Edmondson, D. E.; Mattevi, A. *J. Med. Chem.* **2004**, *47*, 1767.
64. Binda, C.; Newton-Vinson, P.; Hublek, F.; Edmondson, D. E.; Mattevi, A. *Nat. Struct. Biol.* **2002**, *9*, 22.
65. De Colibus, L.; Min, L.; Binda, C.; Lustig, A.; Edmondson, D. E.; Mattevi, A. *Proc. Natl. Acad. Sci. U.S.A.* **2005**, *102*, 12684.
66. Berendsen, H. J. C.; Van der Spoel, D.; Van Drunen, R. *Comput. Phys. Commun.* **1995**, *91*, 56.
67. Lindahl, E.; Hess, B.; Van der Spoel, D. *J. Mol. Model.* **2001**, *7*, 306.
68. Michel, F.; Saner, P. *J. Mol. Graph. Model.* **1999**, *17*, 57.
69. Gasteiger, J.; Marsili, M. *Tetrahedron* **1980**, *36*, 3219.
70. Wavefunction, Inc., 18401 von Karman Avenue, Suite 370, Spartan'02, Irvine, CA 92612, USA.
71. Morris, G. M.; Goodsell, D. S.; Halliday, R. S.; Huey, R.; Hart, W. E.; Belew, R. K.; Olson, A. J. *J. Comput. Chem.* **1998**, *19*, 1639.
72. Huey, R.; Morris, G. M.; Olson, A. J.; Goodsell, D. S. *J. Comput. Chem.* **2007**, *28*, 1145.
73. Toprakçi, M.; Yelekci, K. *Bioorg. Med. Chem. Lett.* **2005**, *15*, 4438.
74. Yelekci, K.; Karahan, O.; Toprakci, M. *J. Neural. Transm.* **2007**, *114*, 725.
75. Humphrey, W.; Dalke, A.; Schulten, K. *J. Mol. Graph.* **1996**, *14*, 33.
76. Lister, R. G. *Psychopharmacology* **1987**, *92*, 10.
77. Porsolt, R. D.; Bertin, A.; Jalfre, M. *Arch. Int. Pharmacod. T.* **1977**, *229*, 327.
78. Lister, R. G. *Psychopharmacology* **1987**, *92*, 180.
79. Pellow, S.; Chopin, P.; File, S. E.; Briley, M. J. *Neurosci. Methods* **1985**, *14*, 149.
80. Porsolt, R. D.; Anton, G.; Blavet, N.; Jalfre, M. *Eur. J. Pharmacol.* **1978**, *47*, 379.